Resource

Cell Reports

Transcriptional and Translational Differences of Microglia from Male and Female Brains

Graphical Abstract

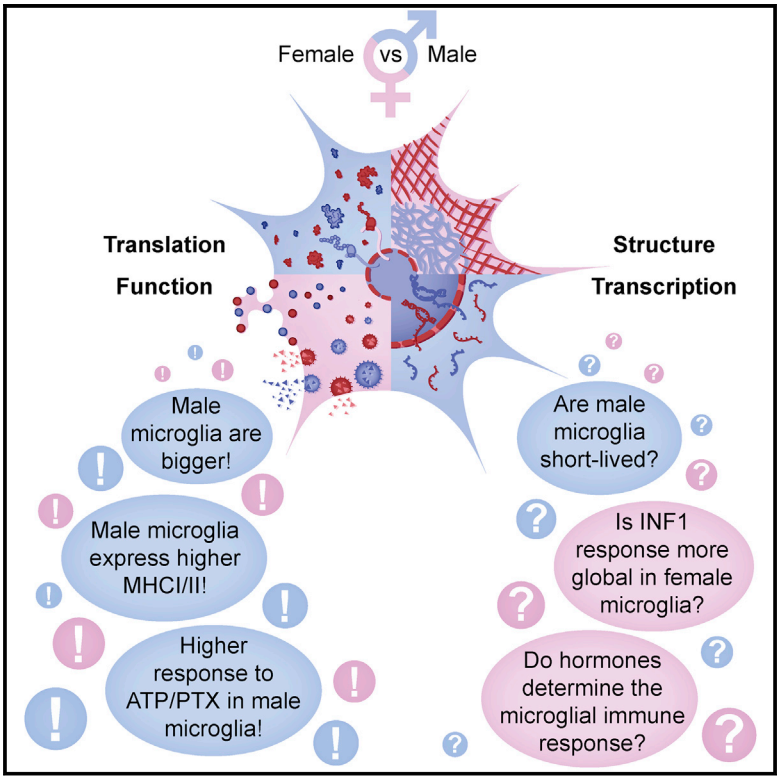

Highlights

- Sex-related differences in key cellular function and parameters in microglia
- Transcriptome of male and female microglia derived from hippocampus and cortex
- Proteomics analysis of male and female microglia from whole brain

Authors

Dilansu Guneykaya, Andranik Ivanov, Daniel Perez Hernandez, ..., Dieter Beule, Helmut Kettenmann, Susanne A. Wolf

Correspondence

susanne.wolf@mdc-berlin.de

In Brief

Guneykaya et al. provide transcriptomic, proteomic, and functional data from male and female microglia, providing a resource for further investigation of sex-based differences in microglia.

Guneykaya et al., 2018, Cell Reports *24*, 2773–2783
September 4, 2018
https://doi.org/10.1016/j.celrep.2018.08.001

CellPress

Cell Reports
Resource

Transcriptional and Translational Differences of Microglia from Male and Female Brains

Dilansu Guneykaya,[1,11] Andranik Ivanov,[2,3,11] Daniel Perez Hernandez,[4,5] Verena Haage,[1] Bartosz Wojtas,[7] Niklas Meyer,[1] Meron Maricos,[1] Philipp Jordan,[1] Alice Buonfiglioli,[1,6] Bartlomiej Gielniewski,[7] Natalia Ochocka,[7] Cagla Cömert,[1] Corinna Friedrich,[4] Lorena Suarez Artiles,[4] Bozena Kaminska,[7] Philipp Mertins,[4,5] Dieter Beule,[2,8] Helmut Kettenmann,[1,11] and Susanne A. Wolf[1,9,10,11,*]

[1]Cellular Neurocience, Max-Delbrueck-Center for Molecular Medicine in the Helmholtz Association, Berlin, Germany
[2]Core Unit Bioinformatics, Berlin Institute of Health, Berlin, Germany
[3]Charité-Universitaetsmedizin, Berlin, Germany
[4]Proteomics Platform, Max-Delbrück-Center for Molecular Medicine in the Helmholtz Association, 13125 Berlin, Germany
[5]Berlin Institute of Health, 13125 Berlin, Germany
[6]Institute of Cell Biology and Neurobiology, Charité-Universitaetsmedizin, Berlin, Germany
[7]Nencki Institute of Experimental Biology of the Polish Academy of Sciences, Warsaw, Poland
[8]Max-Delbrueck-Center for Molecular Medicine in the Helmholtz Association, Berlin, Germany
[9]Department of Ophthalmology, Charité-Universitaetsmedizin, Augustenburger Platz 1, 13353, Berlin, Germany
[10]Present address: Department of Ophthalmology, Charité-Universitaetsmedizin, Augustenburger Platz 1, 13353 Berlin, Germany
[11]These authors contributed equally
*Correspondence: susanne.wolf@mdc-berlin.de
https://doi.org/10.1016/j.celrep.2018.08.001

SUMMARY

Sex differences in brain structure and function are of substantial scientific interest because of sex-related susceptibility to psychiatric and neurological disorders. Neuroinflammation is a common denominator of many of these diseases, and thus microglia, as the brain's immunocompetent cells, have come into focus in sex-specific studies. Here, we show differences in the structure, function, and transcriptomic and proteomic profiles in microglia freshly isolated from male and female mouse brains. We show that male microglia are more frequent in specific brain areas, have a higher antigen-presenting capacity, and appear to have a higher potential to respond to stimuli such as ATP, reflected in higher baseline outward and inward currents and higher protein expression of purinergic receptors. Altogether, we provide a comprehensive resource to generate and validate hypotheses regarding brain sex differences.

INTRODUCTION

In mammals, sex is defined as a combination of direct effects of sex chromosomes Y and X and effects of gonadal hormones, which can be shaped by gene dose and epigenetic processes (Arnold et al., 2012; Dewing et al., 2003). Sex is an important biologic variable in preclinical research (Executive Summary of the Institute of Medicine Report, 2001).

Recognizing this fact is vital because preclinical data inform the premise and design of clinical studies. Historical reliance on male rodents in preclinical research (Zucker and Beery, 2010; Landis et al., 2012) has resulted in the generation of incomplete data available to guide clinical trials that include female participants. This is particularly problematic in view of current knowledge that sex affects health status, including disease presentation, pathophysiology, and therapeutic response. Sex steroids regulate the transcription of genes relevant to the development and maturation of immune cells, immune responses, and immune signaling (van Lunzen and Altfeld, 2014). As a result, the basic inflammatory response differs between the sexes. The exact nature of these differences and how these differences contribute to disease incidence and its progression are quite complex, depending on a multitude of factors, including age, genetics, and environment. In brain diseases involving an inflammatory component, the microglial cells—the brain resident macrophages and phagocytes—play a pivotal role (Wolf et al., 2017).

Microglia influence brain development, including sexual differentiation (Schafer et al., 2013; Lenz and McCarthy, 2015; Garden and Campbell, 2016). Recent evidence has demonstrated that microglia differ in quantity and phenotype between female and male rodents in some regions of the brain, including hippocampus (Mouton et al., 2002; Schwarz et al., 2012; Lenz et al., 2013; McCarthy et al., 2015). It was also shown that masculinization of the brain is dependent upon microglial activation (Lenz et al., 2013; Welberg 2013). Several studies investigated the sex difference in response to the immunomodulatory lipopolysaccharide (LPS) of male and female microglia *in vitro* and *in vivo* (Hanamsagar et al., 2017). Hanamsagar et al. (2017) recently reported transcriptomic data of isolated male and female hippocampal microglia derived from different developmental stages up to P60. It was also shown that the absence of the microbiome has a sex- and time-specific impact on microglia (Thion et al., 2018). Although global transcriptome analysis is a powerful technique that can reveal insights into a phenotype of a given cell, organ or region, RNA levels of a given gene may differ from the protein expression and eventually might only partially reflect

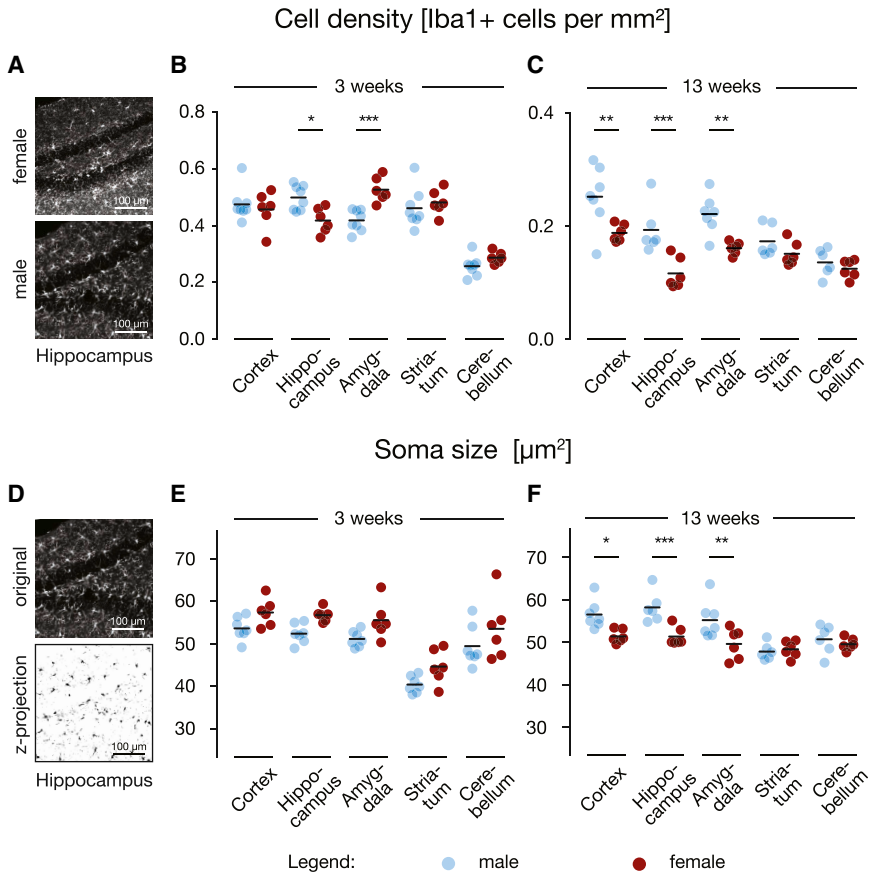

Figure 1. Sex-Dependent Density and Soma Size

(A) Representative fluorescence images of Iba1 labeling to identify microglia in coronal slices from male and female hippocampi (13 weeks old) used to determine microglia cell density.

(B) Microglia density values obtained from brain slices of 3-week-old male and female animals are given for the different brain regions as indicated. Microglia density is significantly higher in the hippocampus and lower in the amygdala in males compared to females (male, n = 6, female, n = 6).

(C) Microglia density values obtained from brain slices of 13-week-old male compared to female mice. Iba1$^+$ cell density in hippocampus, cortex, and amygdala is higher in male versus female mice. No significant changes were observed in striatum and cerebellum at both developmental stages (male, n = 6; female, n = 6).

(D) Top: as an example to illustrate how we prepared the images for soma size analysis, we show here the representative image from panel A (hippocampus, male, 13 weeks old) again. Bottom: Z projection of stack images were set to threshold in order to calculate the soma size. Measures were taken by the software Image J (version 1.51m9).

(E) Average soma size of brain slices obtained from different regions of 3-week-old animals as indicated. No significant differences were observed.

(F) Average soma size of 13-week-old animals. The soma size is larger in male microglia from hippocampus, cortex, and amygdala compared with female mice.

Two-way ANOVA followed by Bonferroni post hoc test; *$p < 0.05$, **$p < 0.01$, and ***$p < 0.001$ were performed. Asterisk indicates significant differences between male and female. Scale bar, 100 µm.

the functional phenotype of a cell (Jovanovic et al., 2015; Schwanhäusser et al., 2011). The predictive value of transcript expression for corresponding proteins is variable in human brain samples, reflecting the complex regulation of protein expression (Bauernfeind and Babbitt, 2017). We therefore provide here structural, functional, transcriptomic, and proteomic data from freshly isolated microglia derived from adult (13 weeks old) brains of male and female mice. Where feasible, we analyzed hippocampal and cortical microglia separately to capture the known brain region specificity.

RESULTS

Sex-Specific Structural Differences

Microglial Cell Density Differs between Male and Female Microglia Depending on Brain Regions

To characterize the effect of sex on microglia density, we labeled these cells with anti-Iba1 (ionized calcium-binding adaptor molecule 1) antibody and compared male and female mice at 3 and 13 weeks of age in five different brain regions: cortex, hippocampus, amygdala, striatum, and cerebellum (representative micrographs for hippocampus in Figure 1A). In 3-week-old males, microglia density in the hippocampus (as determined in a defined plane) was significantly decreased, whereas it was increased in the amygdala compared with females (Figure 1B, male versus female, 1-way ANOVA, $F[4, 60] = 7.199$, $p < 0.0001$). Several structures, such as cortex, striatum, and cerebellum, did not show any differences in microglia density between males and females. In 13-week-old males, density of microglia in the cortex, hippocampus, and amygdala was significantly higher compared with female mice (Figure 1C, male versus female, 1-way ANOVA, $F[1, 52] = 35.56$, $p < 0.0001$), while there was no difference in the striatum and cerebellum.

Soma Size Differs between Male and Female Microglia

Furthermore, we analyzed the soma size at both developmental stages in the five brain regions described above (representative micrographs in Figure 1D). We did not observe significant differences between 3-week-old males and females (Figure 1E). In 13-week-old males, the soma size of microglia was larger in the cortex, hippocampus, and amygdala compared with the females (Figure 1F, male versus female, 1-way ANOVA, $F[1, 52] = 23.9$, $p < 0.0001$), while it was similar in the cerebellum and striatum (Figures 1E and 1F).

Sex-Specific Functional Differences

Microglia Show Sex-Dependent Differences in Their Basic Membrane Properties

To compare the basic membrane properties between male and female microglia, we recorded membrane currents from microglial cells in acute brain slices of the somatosensory cortex

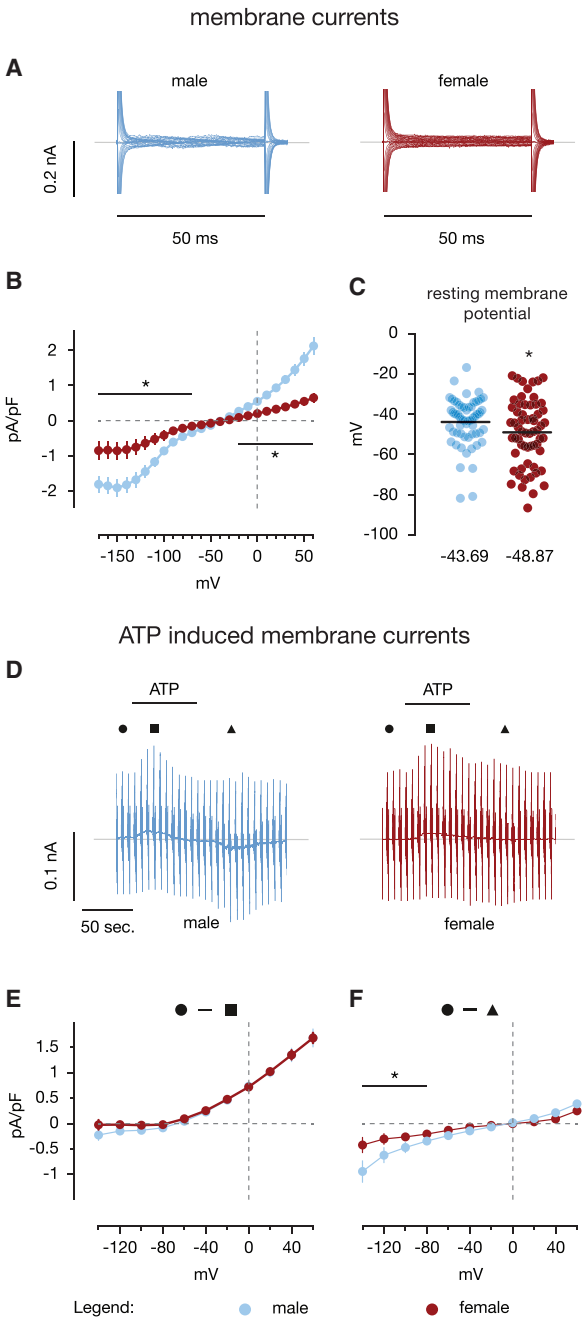

Figure 2. Sex-Dependent Membrane Properties

(A) Membrane currents recorded from microglia located in layers 2–6 of the somatosensory cortex in acute slices. The membrane was clamped to potentials between −170 and 60 mV in 10 mV increments from a holding potential of −70 mV, with duration of 50 ms for each pulse. Microglia were identified by their intrinsic GFP fluorescence under the Csf1R promoter.

(B) The graph illustrates the average current density (pA/pF) to voltage (mV) relationship obtained from 123 microglial cells. Microglia derived from male mice show significantly higher baseline inward and outward conductance compared with female mice ($p < 0.05$ between −170 and −70 and between −20 and +60 mV).

(C) Distribution of reversal potentials from male (n = 61) and female (n = 62) microglial cells. Microglial cells derived from female mice showed a significantly lower reversal potential compared with male mice ($p = 0.048$). Average values indicated at the bottom.

(D) ATP-induced membrane currents were recorded while clamping the membrane every 5 s to a series of de- and hyperpolarizing voltage steps ranging from −140 to +60 mV in 20 mV increments, 100 ms in duration. ATP (1 mM) was applied via the bathing chamber for 1 min as indicated by the bar.

(E) To construct the current density-to-voltage relationship (pA/pF to mV) of the ATP-activated current component, values before ATP application (● filled circles) were subtracted from currents at the peak of the response of the induced inward current (■ filled squares) and the peak of the induced outward current (▲ filled triangles) as indicated in the recording in (D). No significant differences in the reversal potential were observed between sexes concerning outward conductance upon ATP application.

(F) Microglia derived from male mice showed a significantly higher inward conductance compared with female at the voltage steps between −140 and −80 mV ($p < 0.05$).

At least three animals per group were used, and the number of recorded microglia was 28 for males and 19 for females (Student's t test with Welch's correction, $^*p < 0.05$).

(layers 2–6) and the hippocampus using the patch-clamp technique. The microglial cells were identified by green fluorescence in the transgenic Csf1R-EGFP mouse line (Sasmono et al., 2003).

Figure 2A shows representative current profiles of a female and male microglia from cortex. On the basis of these recordings, we determined the current density-to-voltage relationship of the measured inward and outward currents (Figure 2B). It is apparent that male microglia display significantly higher baseline inward and outward conductance ($p < 0.05$). Furthermore, microglia derived from female mice showed a significantly lower reversal potential, which is indicative of the resting membrane potential (Student's t test with Welch's correction; males: −43.69 mV, SEM = 1.511, n = 61; females: −48.87 mV, SEM = 2.098, n = 61; $p = 0.047$) (Figures 2C and S1E).

We did not observed differences between cortical microglia derived from male or female mice in membrane capacitance (Figures S1D and S1E, top) or in membrane resistance of the patched cells (Figure S1F, top). By taking the changes in the reversal potential into account, both findings indicate a differential resting state for male and female cortical microglia.

Differences in the Electrophysiological Response to ATP in Male versus Female Microglia

We tested purinergic signaling by recording membrane current responses to application of ATP in microglial cells from acutely isolated cortical and hippocampal brain slices. As previously described, ATP triggered increases in inward and outward currents with different kinetics and varying frequency (Figure 2D; Boucsein et al., 2000). ATP-induced outwardly rectifying currents were consistently observed and not different in male and female microglia. They had similar reversal potentials close to the K^+ equilibrium potential, indicative of an activation of a K^+ conductance (Figure 2E).

Inward currents often occurred with a delay and were more frequently observed in male compared with female cortical microglia. In male microglia, 16 of 27 cells (59%) showed this response, while in female microglia, 8 of 19 cells showed such a response (42%). These currents had a reversal potential of about 0 mV and an average amplitude measured between voltage steps −80 to −140 mV of 0.970 pA/pF (SEM = 0.210)

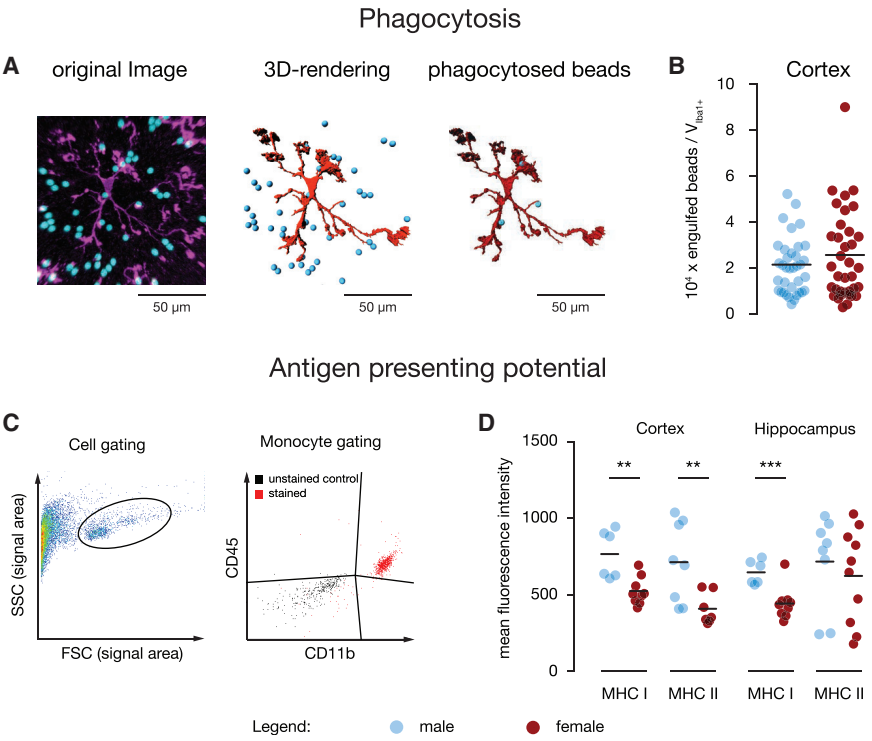

Figure 3. Sex-Dependent Phagocytosis and Antigen-Presenting Potential

(A) Representative confocal images of the phagocytosis assay showing Iba1-stained microglia (magenta) together with latex beads (cyan) in cortical slices. All beads (blue) having their centers located within a given rendered Iba1 volume (red) were considered to be phagocytosed by microglia. The phagocytic index was calculated as followed: $n_{PM} \times 10^4 / V_{Iba\text{-}1}$, where n_{PM} is the total number of phagocytosed microspheres and $V_{Iba\text{-}1}$ the Imaris-rendered volume of Iba1 fluorescence in cubic micrometers.

(B) The microglia phagocytic index was not significantly different in male and female mice (n = 3 animals for each group, one-way ANOVA followed by a post hoc Tukey test for multiple comparisons).

(C) Gating strategy for microglial cell analysis by FACS shown as density plots. The cell populations were gated according to $CD11b^+/CD45^{low}$ expression (microglia). FSC, forward scatter; SSC, sideward scatter.

(D) Mean fluorescence intensity of MHCI and MHCII of microglia ($CD11b^+/CD45^{low}$) from the cortex and hippocampus. MHCI was expressed at a significantly higher level in both regions, and MHCII was only higher in male cortex.

n = 6 male mice, n = 9 female mice; Student's t test: *p < 0.05, **p < 0.01, and ***p < 0.001.

in males and −0.450 pA/pF (SEM = 0.148) in females (Student's t test with Welch's correction; $p < 0.05$, between voltage steps between −140 and −80 mV; Figure 2F). On the basis of their delay, these delayed activated currents are most likely due to P2X7 activation on microglia (Ousingsawat et al., 2015). These findings suggest different functional expression of the P2X system between male and female microglia in the cortical region.

In hippocampal acute slices, we observed no difference in the passive membrane properties (Figures S1A, S1B, and S1D–S1F, bottom) or in P2X- or P2Y-mediated membrane current changes (Figure S1C) between male and female microglia.

Basal In Situ *Phagocytosis Is Similar in Male and Female Microglia*

Another important function of microglia is their phagocytic activity. Therefore, we quantified the engulfment of fluorescent beads by microglia on acute brain slices. We compared the phagocytic activity of microglia in cortical slices of 13-week-old male and female mice. We used the previously established *in situ* phagocytosis assay analyzed by confocal microscopy and three-dimensional (3D) reconstruction, which allowed us to calculate the baseline phagocytic index of microglia (Figure 3A; Video S1). As shown in Figure 3B, baseline microglial phagocytosis index was not different between males and females in cortical slices. The same was true for the phagocytosis activity of microglia in hippocampal slices (data not shown).

Male Microglia Show Higher Antigen-Presenting Potential

Microglia are the major immune cell population in the brain, which processes and presents antigen peptides via major histocompatibility complex (MHC) molecules. We investigated the antigen-presenting potential of microglia freshly isolated from male and female cortex and hippocampus using flow cytometry. The dye-coupled monoclonal anti-mouse antibodies against CD45 and CD11b served to identify microglia as $CD11b^+$, $CD45^{low}$ cells (Figure 3C). In this population, we characterized the expression of MHCI and MHCII. MHCI expression was higher in male microglia in cortex and hippocampus (Figure 3D; Student's t test, male versus female, hippocampus: 645.3 ± 31.72 versus 442.1 ± 35.74; cortex: 752.2 ± 64.85 versus 506.8 ± 30.28). Higher MHCII expression in male microglia was observed only in the cortex (Figure 3D; Student's t test, male versus female, cortex: 698.5 ± 92.74 versus 390.6 ± 39.29). Altogether, our data suggest that naive male microglia have a higher antigen-presenting capacity.

Sex-Specific Transcriptional Difference

Here we compared the transcriptomic profile of freshly isolated microglia from male and female hippocampus and cortex. Using next-generation sequencing, we sequenced polyA-selected mRNAs from microglia isolated from hippocampus and frontal lobe with four replicates for females and three replicates for males. In total ~223.2 million paired end reads with 82%–95% unique fragment mappability were generated. We found good reproducibility between the replicates (Figure S2A). Principal-components analysis (PCA) showed a very clear separation of expression between the two brain regions and the two sexes (Figure S2C).

First, we noted that there was quite a difference in the expression profile in males and females between the two brain regions. We found 1,109 genes differentially expressed between males

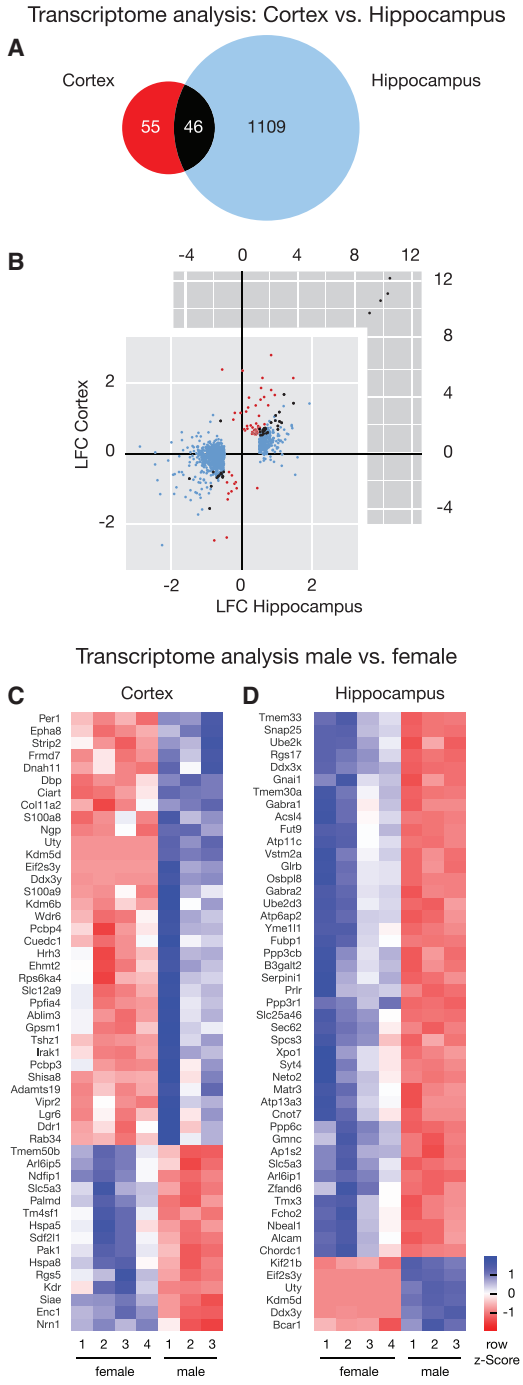

Figure 4. Sex-Dependent Transcriptome Profile

Differential mRNA expression levels between male (n = 3) and female (n = 4) mice in the cortex and hippocampus (n = 3 or 4). For each n cells from 3 animals were pooled (9 males, 12 females).

(A) Venn diagram shows the number of significantly differentially regulated genes (adjusted $p < 0.01$, $|\log_2$ fold change (LFC)$| > 0.5$). We detected about 10times more significantly differentially regulated genes in hippocampus (1,155) compared with frontal lobe (101); the LFCs of these genes show high correlation between the two brain regions (Pearson's correlation coefficient = 0.78).

(B) Scatterplots show the LFCs in male versus female mice for all genes presented in the Venn diagram. In the scatterplot in front, the red dots correspond to the genes differentially regulated in the cortex, blue dots represent the genes differentially regulated in the hippocampus, and black dots represent the genes differentially regulated between males and females in both brain regions. The scatterplot in the back shows four Y-linked genes in the upper right corner that belong to the category "differentially regulated in both brain regions" (black dots). In order to show both the Y-linked genes in the back and all the other differentially regulated genes in the front, we zoomed in the foremost scatterplot for better visibility.

(C and D) The heatmaps represent a subsection of the genes shown in (B). They show the top 50 (sorted by adjusted p value) differentially expressed genes between male and female mice in the cortex (C) and hippocampus (D). Z scores are calculated from gene transcript per million (TPM) values (upregulation in blue, downregulation in red, neutral in white).

and females exclusively in hippocampus and 55 genes differentially expressed exclusively in the cortex, whereas 46 genes were differentially regulated in both regions between males and females (Figure 4A; adjusted $p < 0.01$, $|\log_2$ fold change (LFC)$| > 0.5$). The scatterplot shows a high correlation of sex-specific fold changes in the two regions (Figure 4B, plot in front). The four Y chromosome-specific genes show the high dynamic range of our data (Figure 4B, plot in back).

For the cortex, we detected 72 genes expressed at a higher level and 27 expressed at a lower level in male compared with female microglia. In the hippocampus, the difference in the transcriptomic profile was much more pronounced, and we found 324 genes expressed at a higher level and 867 genes at a lower level in male compared with female microglia. The heatmaps (Figures 4C and 4D) show the top 50 differentially regulated genes between male and female microglia for both regions. We also confirmed our transcriptomic data with qRT-PCR from an additional ten animals with five selected differentially expressed genes in hippocampus and cortex (Figure S2D).

To identify the biological processes differentially regulated in both sexes, we subjected the genes expressed at higher and at lower levels to Gene Ontology (GO) analysis. In the cortex, we restricted the GO enrichment analysis only to the genes expressed at higher levels in males because of the small number of lower expressed genes. In male microglia, "transcription factor activity" (GO 0000982, 989, 977) and "histone demethylation and deacetylation" (GO 0071557/8 and GO 0016575) were among the 30 GO terms overrepresented in the genes expressed at higher levels in the cortex (Figure 5A). The GO analysis of microglia from hippocampus revealed among others the following GO terms overrepresented in the genes expressed at higher levels in male microglia: "regulation of defense response to bacteria" (GO 1900424), "insulin receptor pathway" (GO 0008286), and "glia cell differentiation" (GO 0010001) as well as "ATP binding" (GO 0005524) (Figure 5B). The GO terms "GABA and Glutamate receptor activity" (GO 0007214/5 and 0004890), "ubiquitin protein activity" (GO 006130/1) and "magnesium ion transport" (GO 0015095/15693) were overrepresented in the female microglia gene set (Figure S3A). For the complete datasets, see Table S1.

Because a transcriptomic profile of male versus female hippocampal microglia was recently published for P60 (Hanamsagar et al., 2017), we took the opportunity to add another developmental time point. We found a strong correlation between our 13-week-old mice/microglia (polyA-enriched mRNAs) and the

Figure 5. Gene Ontology Enrichment Analysis of Genes Expressed at Higher Levels in Males

(A and B) Significantly enriched Gene Ontology (GO) terms for the cortex (A) and hippocampus (B) of genes expressed at higher levels in males compared with females: the top 15 molecular functions and top 15 biological processes are shown. The size of the circle represents the number of significantly differentially regulated genes (adjusted $p < 0.01$, $|\log_2 \text{fold change}| > 0.5$) in that GO category. The x axis represents the ratio between significantly differentially regulated genes in the respective gene set measured by sequencing and the total number of genes belonging in that GO category. The larger the number, the more genes belonging to a given GO category were captured in our analysis. The color of the circle represents the p value from 10^{-2} (red) to 10^{-4} (blue).

published P60 data (total RNA), with a correlation coefficient of 0.79 for male hippocampal microglia (Figure S4A). About 1,500 protein coding genes were detected with more than a 16-fold difference between the two experimental approaches. It is possible that some of the differences stem from technical or actual biological differences. To further evaluate the two datasets, we analyzed the length distribution and functions of the genes that differ between the two datasets. Figure S4B shows that the polyA-exclusive genes (dark blue) form longer transcripts. GO terms overrepresented in the genes expressed at a higher level in 13 weeks versus P60 related these changes among others to the GO terms "startle response," "learning," "memory," and "synaptic plasticity" (Figure S4C).

Finally, we also analyzed the transcriptomic differences between hippocampus- and cortex-derived microglia in males and females separately. We expected a regional difference to dominate over sex differences. In the heatmaps (Figures S3B and S3C), we show the 50 most significant differential regulated genes in male and in female microglia derived from cortex and hippocampus. More than half of the genes (64%) came up in both male and female datasets (e.g., *c1qc2*, *sema5a*, *gpr161*, *prox1*), showing the similarity in the transcriptomic profile. In addition, when we performed GO enrichment analysis, we found that 30%–50% of the significant GO terms are the same (data not shown) for both sexes, in accordance with our expectations.

Sex-Specific Translational Difference

To determine the steady-state protein levels in microglia from both sexes, we estimated protein composition of the microglial cells by mass spectrometry (MS)-based proteomics and label-free quantification (LFQ) analysis. We analyzed the differences of protein abundance, comparing the normalized intensity on distinct proteins from four different samples per group. We pooled ~500,000 microglial cells from three brains in order to obtain enough material for MS for one sample. Because of the lower sensitivity of proteomics versus genomics applications, microglia cells taken from the whole brain were analyzed. Therefore, we could perform the proteomic analysis only on whole-brain microglia. We identified 5,500 proteins per sample on average in a single-shot analysis. In total there were 6,208 proteins identified among all samples. We performed quantification in a label-free format using the Max Quant algorithms, using the normalized intensity values (LFQ intensity). We included only proteins that were quantified in at least three experiments in one condition. Analysis of the MS data resulted in 4,627 proteins for statistical quantification. Pairwise comparison of all the samples against each other resulted in high Pearson coefficients, indicating high quantitative accuracy between samples (Figure S2A).

Applying Student's t test comparison, 268 proteins were found to be expressed at significantly higher levels in male microglia and 96 proteins at significantly higher levels in female microglia derived from whole brain (almost 10% of the dataset) (Table S2; adjusted $p < 0.01$, $|\text{LFC}| > 1$).

The heatmap shows genes (Figure 6A) and the table presents respective GO terms overrepresented in the proteins expressed

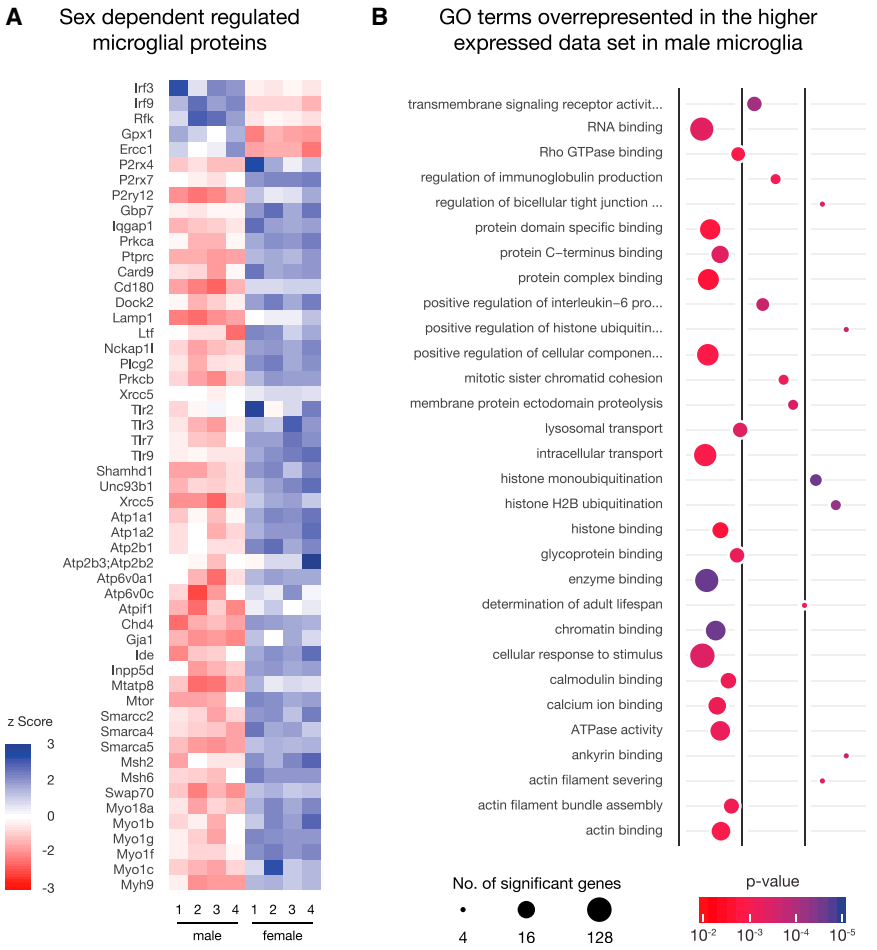

Figure 6. Sex-Dependent Proteome Profile

(A) The heatmap shows selected significantly differentially expressed proteins between male and female microglia (two-tailed Student's t test, false discovery rate < 1%, S_0 = 2, n = 4, each n pools of four brains). The rows represent the 4 samples for male (left) and female (right) microglia pooled from four individual mice each. The *Z* score represents the different regulation, with blue indicating upregulation and red indicating downregulation of genes. Notably more proteins were expressed at higher levels in the male dataset.

(B) Significantly enriched Gene Ontology (GO) terms: top 15 most significant molecular functions and top 15 biological processes. The size of the circle represents the number of significantly differentially regulated genes (4–128, adjusted p < 0.01, $|\log_2$ fold change$| > 0.5$) in that GO category. The color of the circle represents the p value from 10^{-2} (red) to 10^{-5} (blue). The x axis represents the ratio between significantly differentially regulated genes in the respective gene set measured by sequencing and the total number of genes belonging in that GO category.

at higher levels (Figure 6B), which supports some of the functional data shown in Figures 1, 2, and 3. STRING pathway analysis of the proteins with a higher expression level in male microglia revealed that they belong to interconnected pathways implicated into regulation of cellular functions (Figure S5A). A number of proteins highly expressed in male microglia are myosin related (Myh14, Myh9, Myo18a, Myo1b, Myo1c, Myo1f, and Myo1g) proteins that contribute to cell stability, trafficking, shape, and size. This might be reflected on a phenotypic level by the increase in soma size of male microglia (Figures 1E and 1F) and higher motility as shown by others (Yanguas-Casás et al., 2018). We also found P2X purinoceptors 4 and 7 and P2Y purinoceptor 12 (P2RX7, P2RX4, and P2YR12, respectively), which are related to purinergic receptor signaling and mediate current responses to ATP, expressed at significantly higher levels in male microglia. The electrophysiological recordings suggest that the P2Y7-mediated response to ATP is more pronounced in male microglia. We also found proteins related with Toll-like receptor (TLR) pathways expressed at higher levels in male microglia such as TLR2, 3, 7, 9, S100a8 and S100a9, Prkdc, and Xrccr5, which suggest higher responsiveness of male microglia to immunological stimuli. One of the proteins enriched in female microglia was Irf3, which would hint toward a higher potential to respond to and activate type I interferon (IFN-alpha and IFN-beta) related processes. Moreover, other proteins of the same pathway are expressed at higher levels in male microglia (Prkdc and Xrccr5; pathway analysis, Figure S5B). Taken together this might be a prominent example that differences in male and female microglia can originate from a different temporal expression of molecules belonging to the same pathway (Figure S5C).

The differentially expressed proteins were used for further GO analysis (Table S3).

How Are the Functional Differences between Male and Female Microglia Reflected in Their Transcriptomic and Proteomic Profiles?

Because we had the chance to perform transcriptomic and proteomic analysis within the same experimental setting using the same strain of mice, we felt confident to analyze how much they are reflected within each other. Because of technical and logistic limitations (cell number required for proteomics versus cell number required for transcriptomics), we performed proteomics from whole brain and transcriptomics from hippocampus and medial prefrontal cortex separately. We sought to investigate whether the differences in the sex-specific RNA signature of either brain region would also be reflected in the sex-specific whole-brain proteomic profiles. Although technical replicates for both RNA and protein datasets correlated highly, we could not find a striking correlation between the datasets (Figure S2A). A search of GO terms and genes and proteins within the datasets revealed only a few common ones in the proteomic and transcriptomic analysis. For example, the GO term "Rho GTPase

binding'' (GO 0017048) was overrepresented in the dataset from male microglia proteome and male microglia hippocampal transcriptome. Also, one Y-linked gene, *Ddx3y* (DEAD-box helicase 3, Y-linked), was at a higher expression level in the male transcriptome of both cortical and hippocampal microglia and in the male proteome of whole-brain microglia, confirming its microglial origin in males. When we compared the top 30 genes with higher expression levels in male microglia in the proteomics and transcriptomic analysis, we found S100a8 at a higher level in both male microglia proteome and male microglia cortical transcriptome. Pkn1 was found to be at a higher level in the male proteome and in male hippocampal and cortical transcriptome. However, most of the genes and proteins and GO terms were only present either in the proteome or the transcriptome dataset and did not show up in both datasets at all. In addition, we isolated CD11b cells from the whole brain and performed RNA sequencing. However, the correlation between transcriptome and proteome was equally low comparing whole-brain microglia mRNA and protein profile (data not shown). The purity of the isolated cells was tested using CD11b, CD45, Ly6G, and Ly6C labeling and fluorescence-activated cell sorting (FACS) analysis (gating strategy, Figure S6). We monitored gene expression values in different cell-type specific modules defined by Friedman et al. (2018), and our dataset revealed a high correlation only in the microglia module (Table S1; Figure S2B). This was confirmed by an independent FACS analysis: only approximately 0.5%–1.8% of the CD11b population also expressed Ly6G, which is a neutrophil marker (Figure S6B). In conclusion, the contamination rate was very low in all the samples from males and females alike. We therefore conclude that the differences between male and female datasets are indeed based on the 98% CD11b-positive microglial population.

DISCUSSION

In the present study, we aimed to provide a comprehensive overview of the transcriptomic and proteomic profiles of male and female microglia and compare them with cellular characteristics and function. We provide a comprehensive data source to the scientific community for future studies in this field.

Overall, male microglia are more frequent in specific brain areas such as the hippocampus and cortex at 3 and 13 weeks, have bigger somata at 13 weeks, and appear to be more responsive to stimuli or ''ready to go.'' This is reflected for example by a higher expression of MHCI and MHCII on cortical and hippocampal male microglia. Moreover, male microglia had higher baseline outward and inward currents as well as a higher response to ATP in a P2X-dependent manner measured in cortical slices. In addition, proteomic analysis of whole-brain microglia revealed a higher expression of the P2X4, P2X7, and P2Y12 receptors in males.

A few studies have addressed sex differences in microglia density in different brain regions. Schwarz and Bilbo (2012) reported that female Sprague-Dawley rats have higher number of microglia in juvenile and adult stages. On the contrary, Acaz-Fonseca et al. (2015) indicated that females have lower density of Iba1$^+$ cells with a nonreactive morphology in the cortical brain injury mouse model. We show that in the healthy brain, microglia density is increased in male hippocampus at both developmental stages (3 and 13 weeks). These data indicate that the sex difference in microglia density and soma size is dependent upon brain region, age, and species.

Microglial phagocytic activity was previously shown to be more pronounced in female compared with male mice at P0 in hippocampus (Nelson et al., 2017). Perez-Pouchoulen et al. (2015) also suggested that there was no sex difference in frequency of phagocytic cups in the cerebellar layers at the P17 developmental stage. We show that the phagocytic activity of microglial cells in the adult brain was not different between males and females, indicating that microglial phagocytosis is constant after P17 or at least in adult males and females. Microglia expresse several P2Y receptors, which are involved in phagocytosis and motility (Hidetoshi et al., 2012). Phagocytosis is controlled by P2Y6 receptor signaling, which was not differently expressed between male and female microglia. In contrast, P2Y12 receptor expression, which controls microglia motility (Wu et al., 2007), was expressed at a higher level in males compared with females in the proteomics analysis, implying that male microglia may have higher motility capacity. ATP stimulation triggered larger inward K^+ currents in male microglia, which indicates enhanced P2X receptor-mediated signaling. Indeed, proteomic analysis showed that P2X4 and P2X7 receptors are highly expressed in male microglia compared with female. A very recent study showed that female microglia display a neuroprotective phenotype and that transplanted female microglia protected male brains from ischemic stroke (Villa et al., 2018). This is in line with our finding that male microglia seem to be more reactive already under physiological conditions.

One such example is the higher baseline level of S100a8 in male microglia in both datasets (mRNA in the cortex, protein in whole brain). S100a8 is a calcium- and zinc-binding protein, which plays a prominent role in the regulation of inflammatory processes and immune response. In microglia, S100a8/a9 is known to be a TLR4-binding protein and regulates the secretion of pro-inflammatory cytokines (Ma et al., 2017). Dysregulation of S100a8/a9 on microglia has been shown in different disease conditions (Erny et al., 2015; Foster et al., 2006; Gonzalez-Pena et al., 2016), indicating that S100a8/a9 is expressed by microglia and of functional importance. Interestingly a recent study using micro array on microglia isolated from adult C57BL/6 mice showed higher expression of S100a8 mRNA in females (Thion et al., 2018). The isolation and sorting of the cells was different (FACS versus magnetic-activated cell sorting [MACS] in our study) as well as RNA isolation and preparation. More important, the authors discuss that sexual dimorphism in adult microglia showed some variability across housing facilities within their own study. This highlights the importance of the microbiome as a microglia-modulating factor, as they demonstrate in their study.

Pattern recognition molecules such as TLR2, 3, 7, and 9 are higher expressed in male versus female microglia, as revealed by the proteomics analysis, but did not show up in the transcriptomic analysis. We showed by FACS analysis that MHCI and II are highly expressed on male microglia. The MHC expression modulations were not present in proteomic or transcriptomic analysis. On the RNA level, we showed enrichment of genes in

the male dataset that belong to biological processes such as transcription factor activity, histone demethylation, and deacetylation as well as ATP binding and regulation of defense response to bacteria. Our combined findings from proteome, transcriptome, and functional analyses support the previously reported findings of higher immune response of male microglia after an immune challenge with LPS (Loram et al., 2012). On the other hand, we found indications toward a shorter lifespan of male microglia related to the higher expression of Inpp5d and mTOR (GO term "determination of adult lifespan") paralleled by lower expression of Ercc1 both found in the proteomic dataset. This might be in line with the reported developmental index of microglia on the basis of transcriptomic data, where male microglia are described as developmentally delayed compared with female microglia (Hanamsagar et al., 2017). Here we propose that the suggested delayed developmental program in male microglia could also be attributed to a shorter lifespan of these cells.

Although we emphasize here the sex differences, we would like to highlight that similarities with regard to developmental stage and brain regions are also evident and possibly highly conserved between sexes to ensure similar proper functionality of executive processes. More than half of the top 50 genes and 30% of the top 30 GO terms were differentially regulated in both male and female microglia when we compared the brain regions hippocampus and cortex using transcriptomic analysis. When we compared our 13-week dataset with the published P60 dataset of hippocampal male microglia, we found a high correlation between the datasets. However, we also detected a significant number of genes differently regulated. With our conservative cut-off, we identified only 6 significantly differentially regulated genes between males and females in the data set of Hanamsagar et al. (2017) (of which 3 were from *chrY* and 4 had also been identified as differentially expressed in our data). We detected 1,369 genes with 16-fold higher transcripts per million (TPM) in our data, while in the study of Hanamsagar et al. (2017), only 118 were detected. We also detected 138 highly expressed genes in our data that had read counts of zero in P60. In the P60 study, only 2 genes were highly expressed and had no read counts in our study. Noticeably, a major difference between the two experiments is the RNA enrichment/depletion strategy (polyA mRNAs versus total RNA with rRNA depletion). Furthermore, we used paired end sequencing and approximately double the amount of fragments. However, it is likely that the differences between the P60 and 13-week datasets do not stem solely from different protocols and data quality. For example, the GO term "startle response" is overrepresented in the 13-week dataset, and it was shown in behavior studies that the response to a startle is age dependent (Young et al., 2010; Shoji et al., 2016). Moreover, the estrus cycle has an impact on gene expression. Because we did not control for estrus cycle, we cannot rule out that at least part of the difference between the studies could also stem from a different estrus cycle state (Yagi et al., 2017).

When interpreting transcriptomic results, the assumption is frequently made that the expression level of a transcript should correspond to the respective protein level. However, the relationship between these two aspects of molecular phenotype has yet to be fully understood. In fact, the correlation between transcript expression levels and their protein products has generally been found to be quite low and may vary across tissues and cell types (de Sousa Abreu et al., 2009; Maier et al., 2009; Nagaraj et al., 2011; Vogel and Marcotte, 2012; Payne, 2015) and is lowest in the brain (Schwanhäusser et al., 2011).

Proteomic and transcriptomic data are a great resource to test and generate hypotheses. However, functional data are needed to ensure meaningful conclusions. We provide here a sex-specific transcriptomic dataset for hippocampal and cortical microglia as well as a sex-specific proteomic dataset for whole-brain microglia. We also show that our data are a great resource for the scientific community to generate new hypotheses. We have already supported some of these hypotheses with functional and structural data; others will be tested in future studies to explore gender-based therapeutic strategies targeting microglia cells in neuroinflammatory, neurodevelopmental, and neurodegenerative diseases.

STAR★METHODS

Detailed methods are provided in the online version of this paper and include the following:

- KEY RESOURCES TABLE
- CONTACT FOR REAGENT AND RESOURCE SHARING
- EXPERIMENTAL MODEL AND SUBJECT DETAILS
  - Animals
  - Ethics Statement
- METHOD DETAILS
  - Iba1 Immunohistochemistry and confocal microscopy
  - Acute brain slice preparation for electrophysiological recordings
  - Electrophysiological recordings
  - *In situ* phagocytosis assay
  - Flow cytometry analysis
  - Magnetic cell sorting (MACS) of microglial cells
  - Purity analysis of CD11b+ MACS sorted cells using Flow Cytometry
  - mRNA library preparation and sequencing
  - qRT-PCR validation of selected genes
  - Protein extraction and Mass spectrometry analysis
- QUANTIFICATION AND STATISTICAL ANALYSIS
  - Bioinformatic analysis of the RNA seq data
  - Statistical Analysis
- DATA AND SOFTWARE AVAILABILITY

SUPPLEMENTAL INFORMATION

Supplemental Information includes six figures, four tables, and one video and can be found with this article online at https://doi.org/10.1016/j.celrep.2018.08.001.

ACKNOWLEDGMENTS

We thank Julie Colthorpe for proofreading the manuscript. We thank Regina Piske, Nadine Scharek, and Michaela Seeger-Zografski for technical assistance. We thank the microscopy core facility of the Max-Delbrueck-Center (MDC) (Advanced Light Microscopy [ALM]) and FACS facility for technical assistance. We acknowledge the contribution of Dr. Stefan Wendt, who produced the data for the electrophysiology part of the male microglia. The

work was supported by Deutsche Forschungsgemeinschaft (DFG) grant WO 1418/3-1 (to S.A.W.).

AUTHOR CONTRIBUTIONS

Conceptualization, S.A.W., H.K., and D.G.; Software, A.I. and D.P.H.; Formal Analysis, D.G., A.I., D.P.H., N.M., and M.M., Investigation, D.G., A.I., D.P.H., V.H., B.W., N.M., M.M., A.B., B.G., N.O., C.C., C.F., and L.S.A.; Visualization, P.J.; Writing – Original Draft, S.A.W., H.K., and D.G.; Writing – Review & Editing, S.A.W., H.K., D.G., A.I., D.P.H., V.H., B.W., N.M., M.M., A.B., B.K., P.M., and D.B.; Supervision, S.A.W., H.K., B.K., P.M., and D.B.; Project Administration, S.A.W.; Funding Acquisition, S.A.W. and H.K.

DECLARATION OF INTEREST

The authors declare no competing interests.

Received: November 15, 2017
Revised: April 19, 2018
Accepted: July 31, 2018
Published: September 4, 2018

REFERENCES

Acaz-Fonseca, E., Duran, J.C., Carrero, P., Garcia-Segura, L.M., and Arevalo, M.A. (2015). Sex differences in glia reactivity after cortical brain injury. Glia *63*, 1966–1981.

Arnold, A.P., Chen, X., and Itoh, Y. (2012). What a difference an X or Y makes: sex chromosomes, gene dose, and epigenetics in sexual differentiation. Handb. Exp. Pharmacol. *214*, 67–88.

Bauernfeind, A.L., and Babbitt, C.C. (2017). The predictive nature of transcript expression levels on protein expression in adult human brain. BMC Genomics *18*, 322.

Boucsein, C., Kettenmann, H., and Nolte, C. (2000). Electrophysiological properties of microglial cells in normal and pathologic rat brain slices. Eur. J. Neurosci. *12*, 2049–2058.

Boucsein, C., Zacharias, R., Färber, K., Pavlovic, S., Hanisch, U.K., and Kettenmann, H. (2003). Purinergic receptors on microglial cells: functional expression in acute brain slices and modulation of microglial activation in vitro. Eur. J. Neurosci. *17*, 2267–2276.

Cox, J., and Mann, M. (2008). MaxQuant enables high peptide identification rates, individualized p.p.b.-range mass accuracies and proteome-wide protein quantification. Nat. Biotechnol. *26*, 1367–1372.

de Sousa Abreu, R., Penalva, L.O., Marcotte, E.M., and Vogel, C. (2009). Global signatures of protein and mRNA expression levels. Mol. Biosyst. *5*, 1512–1526.

Dewing, P., Shi, T., Horvath, S., and Vilain, E. (2003). Sexually dimorphic gene expression in mouse brain precedes gonadal differentiation. Brain Res. Mol. Brain Res. *118*, 82–90.

Dobin, A., Davis, C.A., Schlesinger, F., Drenkow, J., Zaleski, C., Jha, S., Batut, P., Chaisson, M., and Gingeras, T.R. (2013). STAR: ultrafast universal RNA-seq aligner. Bioinformatics *29*, 15–21.

Endoh, Y., Chung, Y.M., Clark, I.A., Geczy, C.L., and Hsu, K. (2009). IL-10-dependent S100A8 gene induction in monocytes/macrophages by double-stranded RNA. J. Immunol *182*, 2258–2268.

Erny, D., Hrabě de Angelis, A.L., Jaitin, D., Wieghofer, P., Staszewski, O., David, E., Keren-Shaul, H., Mahlakoiv, T., Jakobshagen, K., Buch, T., et al. (2015). Host microbiota constantly control maturation and function of microglia in the CNS. Nat. Neurosci. *18*, 965–977.

Executive Summary of the Institute of Medicine Report (2001). Exploring the biological contributions to human health: does sex matter? J. Womens Health Gend. Based Med. *10*, 433–439.

Fang, M.Z., Zhang, X., and Zarbl, H. (2010). Methylselenocysteine resets the rhythmic expression of circadian and growth-regulatory genes disrupted by nitrosomethylurea in vivo. Cancer Prev. Res. (Phila) *3*, 640–652.

Foster, R., Kandanearatchi, A., Beasley, C., Williams, B., Khan, N., Fagerhol, M.K., and Everall, I.P. (2006). Calprotectin in microglia from frontal cortex is up-regulated in schizophrenia: evidence for an inflammatory process? Eur. J. Neurosci. *24*, 3561–3566.

Friedman, B.A., Srinivasan, K., Ayalon, G., Meilandt, W.J., Lin, H., Huntley, M.A., Cao, Y., Lee, S.H., Haddick, P.C.G., Ngu, H., et al. (2018). Diverse brain myeloid expression profiles reveal distinct microglial activation states and aspects of Alzheimer's disease not evident in mouse models. Cell Rep. *22*, 832–847.

Garden, G.A., and Campbell, B.M. (2016). Glial biomarkers in human central nervous system disease. Glia *64*, 1755–1771.

Gonzalez-Pena, D., Nixon, S.E., O'Connor, J.C., Southey, B.R., Lawson, M.A., McCusker, R.H., Borras, T., Machuca, D., Hernandez, A.G., Dantzer, R., et al. (2016). Microglia transcriptome changes in a model of depressive behavior after immune challenge. PLoS ONE *11*, e0150858.

Hanamsagar, R., Alter, M.D., Block, C.S., Sullivan, H., Bolton, J.L., and Bilbo, S.D. (2017). Generation of a microglial developmental index in mice and in humans reveals a sex difference in maturation and immune reactivity. Glia *65*, 1504–1520.

Hidetoshi, T.-S., Makoto, T., and Inoue, K. (2012). P2Y receptors in microglia and neuroinflammation. Wiley Interdiscip. Rev. Membr. Transp. Signal. *1*, 493–501.

Jovanovic, M., Rooney, M.S., Mertins, P., Przybylski, D., Chevrier, N., Satija, R., Rodriguez, E.H., Fields, A.P., Schwartz, S., Raychowdhury, R., et al. (2015). Immunogenetics. Dynamic profiling of the protein life cycle in response to pathogens. Science *347*, 1259038.

Kanashova, T., Popp, O., Orasche, J., Karg, E., Harndorf, H., Stengel, B., Sklorz, M., Streibel, T., Zimmermann, R., and Dittmar, G. (2015). Differential proteomic analysis of mouse macrophages exposed to adsorbate-loaded heavy fuel oil derived combustion particles using an automated sample-preparation workflow. Anal. Bioanal. Chem. *407*, 5965–5976.

Landis, S.C., Amara, S.G., Asadullah, K., Austin, C.P., Blumenstein, R., Bradley, E.W., Crystal, R.G., Darnell, R.B., Ferrante, R.J., Fillit, H., et al. (2012). A call for transparent reporting to optimize the predictive value of preclinical research. Nature *490*, 187–191.

Lee, H., Ahn, H.H., Lee, W., Oh, Y., Choi, H., Shim, S.M., Shin, J., and Jung, Y.K. (2016). ENC1 modulates the aggregation and neurotoxicity of mutant Huntingtin through p62 under ER stress. Mol. Neurobiol *53*, 6620–6634.

Lenz, K.M., and McCarthy, M.M. (2015). A starring role for microglia in brain sex differences. Neuroscientist *21*, 306–321.

Lenz, K.M., Nugent, B.M., Haliyur, R., and McCarthy, M.M. (2013). Microglia are essential to masculinization of brain and behavior. J. Neurosci. *33*, 2761–2772.

Liao, Y., Smyth, G.K., and Shi, W. (2014). featureCounts: an efficient general purpose program for assigning sequence reads to genomic features. Bioinformatics *30*, 923–930.

Loram, L.C., Sholar, P.W., Taylor, F.R., Wiesler, J.L., Babb, J.A., Strand, K.A., Berkelhammer, D., Day, H.E., Maier, S.F., and Watkins, L.R. (2012). Sex and estradiol influence glial pro-inflammatory responses to lipopolysaccharide in rats. Psychoneuroendocrinology *37*, 1688–1699.

Love, M.I., Huber, W., and Anders, S. (2014). Moderated estimation of fold change and dispersion for RNA-seq data with DESeq2. Genome Biol. *15*, 550.

Ma, L., Sun, P., Zhang, J.C., Zhang, Q., and Yao, S.L. (2017). Proinflammatory effects of S100A8/A9 via TLR4 and RAGE signaling pathways in BV-2 microglial cells. Int. J. Mol. Med. *40*, 31–38.

Maier, T., Güell, M., and Serrano, L. (2009). Correlation of mRNA and protein in complex biological samples. FEBS Lett. *583*, 3966–3973.

McCarthy, M.M., Pickett, L.A., VanRyzin, J.W., and Kight, K.E. (2015). Surprising origins of sex differences in the brain. Horm. Behav. *76*, 3–10.

Mouton, P.R., Long, J.M., Lei, D.L., Howard, V., Jucker, M., Calhoun, M.E., and Ingram, D.K. (2002). Age and gender effects on microglia and astrocyte numbers in brains of mice. Brain Res. *956*, 30–35.

Nagaraj, N., Wisniewski, J.R., Geiger, T., Cox, J., Kircher, M., Kelso, J., Pääbo, S., and Mann, M. (2011). Deep proteome and transcriptome mapping of a human cancer cell line. Mol. Syst. Biol. *7*, 548.

Nelson, L.H., Warden, S., and Lenz, K.M. (2017). Sex differences in microglial phagocytosis in the neonatal hippocampus. Brain Behav. Immun. *64*, 11–22.

Ogoh, H., Tanuma, N., Matsui, Y., Hayakawa, N., Inagaki, A., Sumiyoshi, M., Momoi, Y., Kishimoto, A., Suzuki, M., Sasaki, N., Ohuchi, T., Nomura, M., Teruya, Y., Yasuda, K., Watanabe, T., and Shima, H. (2016). The protein phosphatase 6 catalytic subunit (Ppp6c) is indispensable for proper post-implantation embryogenesis. Mech. Dev *139*, 1–9.

Ousingsawat, J., Wanitchakool, P., Kmit, A., Romao, A.M., Jantarajit, W., Schreiber, R., and Kunzelmann, K. (2015). Anoctamin 6 mediates effects essential for innate immunity downstream of P2X7 receptors in macrophages. Nat. Commun. *6*, 6245.

Payne, S.H. (2015). The utility of protein and mRNA correlation. Trends Biochem. Sci. *40*, 1–3.

Perez-Pouchoulen, M., VanRyzin, J.W., and McCarthy, M.M. (2015). Morphological and phagocytic profile of microglia in the developing rat cerebellum. eNeuro, Published online August 31, 2015. http://doi.org/10.1523/ENEURO.0036-15.2015.

Rappsilber, J., Mann, M., and Ishihama, Y. (2007). Protocol for micro-purification, enrichment, pre-fractionation and storage of peptides for proteomics using StageTips. Nat. Protoc. *2*, 1896–1906.

Sasmono, R.T., Oceandy, D., Pollard, J.W., Tong, W., Pavli, P., Wainwright, B.J., Ostrowski, M.C., Himes, S.R., and Hume, D.A. (2003). A macrophage colony-stimulating factor receptor-green fluorescent protein transgene is expressed throughout the mononuclear phagocyte system of the mouse. Blood *101*, 1155–1163.

Schafer, D.P., Lehrman, E.K., and Stevens, B. (2013). The "quad-partite" synapse: microglia-synapse interactions in the developing and mature CNS. Glia *61*, 24–36.

Schwanhäusser, B., Busse, D., Li, N., Dittmar, G., Schuchhardt, J., Wolf, J., Chen, W., and Selbach, M. (2011). Global quantification of mammalian gene expression control. Nature *473*, 337–342.

Schwarz, J.M., and Bilbo, S.D. (2012). Sex, glia, and development: interactions in health and disease. Horm. Behav. *62*, 243–253.

Schwarz, J.M., Sholar, P.W., and Bilbo, S.D. (2012). Sex differences in microglial colonization of the developing rat brain. J. Neurochem. *120*, 948–963.

Shevchenko, A., Tomas, H., Havlis, J., Olsen, J.V., and Mann, M. (2006). In-gel digestion for mass spectrometric characterization of proteins and proteomes. Nat. Protoc. *1*, 2856–2860.

Shoji, H., Takao, K., Hattori, S., and Miyakawa, T. (2016). Age-related changes in behavior in C57BL/6J mice from young adulthood to middle age. Mol. Brain *9*, 11.

Thion, M.S., Low, D., Silvin, A., Chen, J., Grisel, P., Schulte-Schrepping, J., Blecher, R., Ulas, T., Squarzoni, P., Hoeffel, G., et al. (2018). Microbiome influences prenatal and adult microglia in a sex-specific manner. Cell *172*, 500–516.e16.

Tyanova, S., Temu, T., Sinitcyn, P., Carlson, A., Hein, M.Y., Geiger, T., Mann, M., and Cox, J. (2016). The Perseus computational platform for comprehensive analysis of (prote)omics data. Nat. Methods *13*, 731–740.

van Lunzen, J., and Altfeld, M. (2014). Sex differences in infectious diseases-common but neglected. J. Infect. Dis. *209* (*Suppl 3*), S79–S80.

Villa, A., Gelosa, P., Castiglioni, L., Cimino, M., Rizzi, N., Pepe, G., Lolli, F., Marcello, E., Sironi, L., Vegeto, E., and Maggi, A. (2018). Sex-specific features of microglia from adult mice. Cell Rep. *23*, 3501–3511.

Vogel, C., and Marcotte, E.M. (2012). Insights into the regulation of protein abundance from proteomic and transcriptomic analyses. Nat. Rev. Genet. *13*, 227–232.

Welberg, L. (2013). Microglia maketh the male. Nat. Rev. Neurosci. *14*, 226.

Wendt, S., Maricos, M., Vana, N., Meyer, N., Guneykaya, D., Semtner, M., and Kettenmann, H. (2017). Changes in phagocytosis and potassium channel activity in microglia of 5xFAD mice indicate alterations in purinergic signaling in a mouse model of Alzheimer's disease. Neurobiol. Aging *58*, 41–53.

Wolf, S.A., Boddeke, H.W., and Kettenmann, H. (2017). Microglia in physiology and disease. Annu. Rev. Physiol. *79*, 619–643.

Wu, L.J., Vadakkan, K.I., and Zhuo, M. (2007). ATP-induced chemotaxis of microglial processes requires P2Y receptor-activated initiation of outward potassium currents. Glia *55*, 810–821.

Yagi, S., Drewczynski, D., Wainwright, S.R., Barha, C.K., Hershorn, O., and Galea, L.A.M. (2017). Sex and estrous cycle differences in immediate early gene activation in the hippocampus and the dorsal striatum after the cue competition task. Horm. Behav. *87*, 69–79.

Yanguas-Casás, N., Crespo-Castrillo, A., de Ceballos, M.L., Chowen, J.A., Azcoitia, I., Arevalo, M.A., and Garcia-Segura, L.M. (2018). Sex differences in the phagocytic and migratory activity of microglia and their impairment by palmitic acid. Glia *66*, 522–537.

Young, J.W., Wallace, C.K., Geyer, M.A., and Risbrough, V.B. (2010). Age-associated improvements in cross-modal prepulse inhibition in mice. Behav. Neurosci. *124*, 133–140.

Zucker, I., and Beery, A.K. (2010). Males still dominate animal studies. Nature *465*, 690.

STAR★METHODS

KEY RESOURCES TABLE

REAGENT or RESOURCE	SOURCE	IDENTIFIER
Antibodies		
rabbit anti-Iba1	Wako Pure Chemicals	Cat#019-19741; RRID: AB_839504
donkey anti-rabbit Cy3	Dianova	cat#711-165-152; RRID: AB_2307443
DAPI	Dianova	cat#32670; RRID: AB_2173853
Anti-goat Iba1 antibody	Abcam	Cat#Ab5076; RRID: AB_2224402
Alexa Fluor® 488-donkey anti-goat antibody	Invitrogen/Dianova	705-545-147; RRID: AB_2336933
CD45- eflour 450	eBioscience	Cat#48-0451-82; RRID: AB_1518806
CD11b- PE Cy7	eBioscience	Cat#25-0112-82; RRID: AB_469588
CD11b Monoclonal Antibody (M1/70), Alexa Fluor 700	eBioscience	Cat#56-0112-82; RRID: AB_657585
Anti-Mouse MHCI (H-2Kd/H-2Dd) FITC	eBioscience	Cat#11-5998-81; RRID: AB_465357
MHC Class II (I-A/I-E) (M5/114.15.2), APC-eFluor 780,	eBioscience	Cat#47-5321-82; RRID: AB_1548783
Ly6-G	eBioscience	Cat#12-9668-80; RRID: AB_2572719
Anti-Mouse Ly-6C PerCP-Cyanine5.5	eBioscience	Cat#45-5932-80; RRID: AB_2723342
CD11b magnetic beads	Miltenyi Biotech	Cat#130-093-634
Chemicals, Peptides, and Recombinant Proteins		
FCS-coated Bright Blue fluorescent carboxylated microspheres 4.5 μm diameter	Polysciences	cat#18340-5
Aqua-Poly/Mount	Polysciences	cat#18606-5
Percoll	GE Healthcare	cat#GE17-0891-01
TRIzol	life technologies	10296-028
Critical Commercial Assays		
RNA 6000 Nano LabChip kit	Agilent Technologies	Cat# 5067-1511
KAPA Stranded mRNA Sample Preparation Kit	Kapa Biosystems	Cat# KK8420
cDNA library preparation	NEB	cat#E6100
Agilent DNA High Sensitivity chip	Agilent Technologies	Cat# 5067-4627
QuantiFluor double stranded DNA System	Promega	Cat# E2670
HiSeq 1500	Illumina	Cat# SY-405-1501
Adult Brain Dissociation Kit	Miltenyi Biotech	cat#130-107-677
HTS PAL system	CTC Analytics	https://www.palsystem.com/index.php?id=283
reversed-phase (C18) StageTips	Rappsilber	Rappsilber et al., 2007
nano EasyLC 1200	Thermo Fisher Scientific	cat#LC140
MonoCap C18 HighResolution Ultra column	GL Sciences	cat#5020-10018
Deposited Data		
The accession number for the raw sequencing Data BioProject: PRJNA408225 reported in this paper is:	This paper	ID: SRP118459
The accession number for the mass Spectrometry raw data reported in this paper is:	This paper	ID codes: PXD008114
RNA-Seq male hippocampus, P60	N/A	Hanamsagar et al., 2017
Experimental Models: Organisms/Strains		
Mouse: C57BL/6NCrl	Charles River Laboratories	N/A
Mouse: B6.129P-*Cx3cr1*^{tm1Litt}/J	The *Jackson Laboratory*	Cat#005582; RRID: IMSR_JAX:005582
Oligonucleotides		
S100a8 primer: forward 5′-CCGTCTTCAAGACATCGT TTGA-3′ reverse 5′-GTAGAGGGCATGGTGATTTCCT-3′	Endoh et al., 2009	http://www.jimmunol.org/content/182/4/2258

(*Continued on next page*)

Continued

REAGENT or RESOURCE	SOURCE	IDENTIFIER
S100a9 forward 5′-ATACTCTAGGAAGGAAGGACACC-3′, reverse5′-TCCATGATGTCATTTATGAGGGC-3′	Endoh et al., 2009	http://www.jimmunol.org/content/182/4/2258
Per1 forward 5′-TGGCTGATGACACTGATGCAA-3′, reverse 5′-CTCGTGTCCATTGGATTCATTG-3′	Fang et al., 2010	http://cancerpreventionresearch.aacrjournals.org/content/3/5/640
Enc1 forward 5′-ACCCTGCACGAGTGGTC-3′,reverse 5′-GGACAGGTGGCCGGTACAGT-3′	Lee et al., 2016	https://link.springer.com/article/10.1007%2Fs12035-015-9557-8
Ppp6c forward 5′- ACACAGGTGTATGGATTTTATGATG −3, reverse 5′- TGAGCATATCAAAAACTTTGGTACAG −3′.	Ogoh et al., 2016	https://www.sciencedirect.com/science/article/pii/S0925477316300041#s0010
Software and Algorithms		
LASAF software	Leica Microsystem	https://www.leica-microsystems.com/products/microscope-software/details/product/leica-las-x-ls/
Fiji ImageJ software (1.51m9 64 mb)	NIH	https://imagej.nih.gov/ij/download.html
Imaris 6.3.1	Bitplane	http://www.bitplane.com/releasenotes/imaris631.aspx
GraphPad Prism 6	La Jolla	https://www.graphpad.com/support/prism-6-updates/
Patchers Power Tools	Mendez& Wurriehausen	N/A
Igor Pro 7 software	Wavemetrics	https://www.wavemetrics.com/products/igorpro/newfeatures/whatsnew7.htm
FlowJo v10 software	Tree Star	http://docs.flowjo.com/d2/
R-statistical software package (version 3.4.1)	R Foundation	https://www.r-project.org/
Perseus software (version 1.6.0.7)	Tyanova et al., 2016	N/A
Other		
HM650V vibratome	Thermo Scientific	cat#10076838
EPC9 and EPC10 amplifiers	HEKA Elektronik	N/A
Leica TCS SPE	Leica Microsystem	N/A
LSRII flow cytometer	BD Bioscience	N/A
Orbitrap Q Exactive mass spectrometer	Thermo Fisher Scientific	N/A

CONTACT FOR REAGENT AND RESOURCE SHARING

Further information and requests for resources and reagents should be directed to and will be fulfilled by the Lead Contact, Susanne A. Wolf, PhD (Susanne.wolf@charite.de).

EXPERIMENTAL MODEL AND SUBJECT DETAILS

Animals

All mice used for the present study were on a C57BL/6J genetic background of both sexes and animals were handled according to governmental (LaGeSo) and internal (MDC) rules and regulations. For the electrophysiological study, C57BL/6J background Csf1R-EGFP expression mice were used to allow detection of microglial cells by their fluorescence. The mice were kept in our animal facility with 12 hours of light and dark cycle with food and water *ad libitum*.

Ethics Statement

All procedures involving the handling of living animals were performed in strict accordance with the German Animal Protection Law and were approved by the Regional Office for Health and Social Services in Berlin (Landesamt für Gesundheit und Soziales, Berlin, Germany, Permit Number T0014/08, X9023/12). Adult mice were sacrificed by cervical dislocation or intraperitoneal injection of pentobarbital (Narcoren, Merial GmbH, Hallbergmoos, Germany) for following experiments. All efforts were made to minimize suffering.

METHOD DETAILS

Iba1 Immunohistochemistry and confocal microscopy

Animals were perfused with 1x phosphate buffered saline (PBS) followed by 4% PFA in PBS, decapitated and sectioned in the coronal plane at 40 μm thickness. Free-floating 40μm thick sections were incubated in 5% donkey serum and 0.1% triton-X in tris-buffered saline solution (TBSplus). Iba1 primary antibody was prepared in TBSplus at the following dilution: rabbit anti-Iba1 (Wako chemicals GmbH, Neuss, Germany, product code: 019-19741) 1:400 and sections were incubated with the primary antibodies over-night at 4°C. Secondary antibodies were also prepared in TBSplus at the following dilutions: donkey anti-rabbit Cy3 (Dianova, Hamburg, Germany) 1:200, cell nucleus were stained using 4',6-diamidino-2-phenylindole (DAPI, Dianova, Hamburg, Germany) 1:500 and sections were incubated with secondary antibodies at room temperature for two hours. Images were acquired with a confocal microscope equipped with a 10X objective using LASAF software. Pictures were taken throughout the entire thickness of the slice by Z stack analysis (8 μm z-step size, 10 steps), covering the surface of the respective region. The number of microglia cells per/mm^2 were quantified using Fiji ImageJ software (NIH, Maryland, USA). A total of four slices per animal we sampled for the analysis.

Acute brain slice preparation for electrophysiological recordings

Acute cortical brain slices were prepared as described earlier (Boucsein et al., 2003). In brief, mice were sacrificed by cervical dislocation and the brain was removed and cooled down in ice-cold artificial cerebrospinal fluid (ACSF) containing (in mM): NaCl, 134; KCl, 2.5; $MgCl_2$, 1.3; $CaCl_2$, 2; K_2HPO_4, 1.25; $NaHCO_3$, 26; D-glucose, 10; pH 7.4; gassed with 95% O_2/ 5% CO_2. Brains were mounted on a vibratome (HM650V, Thermo Scientific, Massachusetts, USA) and 250 μm thick coronal brain slices were made and kept at room temperature for experiments for up to 5 h.

Electrophysiological recordings

For electrophysiological recordings, conventional patch-clamp amplifiers were used (EPC9 and EPC10, HEKA Elektronik, Lambrecht, Germany). Microglia in layers 2 – 6 of the somatosensory cortex and the hippocampus were identified by their green fluorescence on an epifluorescent microscope. Patch pipettes were pulled from borosilicate glasses and had resistances of 4 to 6 MΩ. The following intracellular solution was used (in mM): KCl, 130; $MgCl_2$, 2; $CaCl_2$, 0.5; Na-ATP, 2; EGTA, 5; HEPES, 10 and sulforhodamine 101, 0.01 (Sigma Aldrich) and had an osmolarity of 280 - 290 mOsm/L adjusted to a pH of 7.3 with KOH. As extracellular solution the following ACSF was used (in mM): NaCl, 134; KCl, 2.5; $MgCl_2$, 1.3; $CaCl_2$, 2; K_2HPO_4, 1.25; $NaHCO_3$, 26; D-glucose, 10; pH 7.4; with an osmolarity of 310 - 320 mOsm/L and gassed with 95% O_2/ 5% CO_2. Experiments with series resistances less than 50 MΩ were used for data analysis. All experiments were performed in voltage-clamp configuration. To obtain current-voltage curves during continuous recordings, the membrane was clamped every 5 s from a holding potential of 40 mV to a series of de- and hyperpolarizing voltage pulses (100 ms) ranging from −140 mV to +60 mV with 20 mV increments. For evaluation of baseline microglial membrane properties, we clamped the membrane from a holding potential of −70 mV to potentials between −170 mV and +60 mV with 10 mV increments and a duration of 50 ms for each pulse. All currents were online Bessel-filtered at 2.9 kHz. Capacitive transients from the pipette were compensated online via the patch clamp amplifier (Cfast) whereas membrane capacity and series resistance (Cslow) were not compensated. The liquid junction potential between intra- and extracellular solutions was – 3 mV calculated by Patchers Power Tools (Mendez & Wurriehausen, Gottingen, Germany) and Igor Pro 7 software (Wavemetrics, Portland, OR, USA). Membrane capacitance was quantified based on an exponential fit of the current decay in response to a 10 mV test pulse. The same pulse was used to quantify series resistance from the peak amplitude of the membrane capacitance currents. Comparison of membrane currents between different groups were always normalized to the membrane capacitance. The data for male microglia have been published as control for 5xFAD male microglia in a recent paper with focus on Alzheimer's disease (Wendt et al., 2017).

In situ phagocytosis assay

Quantification of microglial phagocytic activity in acute cortical and hippocampal brain slices of 130 μm thickness was conducted in male and female wild-type C57BL/6 mice. We analyzed randomly chosen fields of views from cortical (layers I - II and cortical layers III – VI) and hippocampal areas. 13 week old male and female wild-type C57BL/6 mice were analyzed (n = 3 each sex, respectively). Mice were sacrificed by cervical dislocation and the brain was removed and cooled down in ice-cold artificial cerebrospinal fluid (ACSF) containing (in mM): NaCl, 134; KCl, 2.5; $MgCl_2$, 1.3; $CaCl_2$, 2; K_2HPO_4, 1.25; $NaHCO_3$, 26; D-glucose, 10; pH 7.4; gassed with 95% O_2/ 5% CO_2. Brains were mounted on a vibratome (HM650V, Thermo Scientific, Massachusetts, USA) and 130 μm thick coronal brain slices were sliced. After dissection, cortical sections were kept at room temperature for experiments for 2 h. Next, acute brain slices were incubated with a suspension of FCS-coated Bright Blue fluorescent carboxylated microspheres (4.5 μm diameter, Polysciences). Prior to incubation, the bright blue fluorescent carboxylated microspheres were opsonized with FCS by shaking at 1,000 rpm (Eppendorf Centrifuge 5417R- Rotor FA45-30-11; rotor radius metric: 9.5 cm) for 30 min at RT. After centrifugation of opsonized beads for 2 min at 3,000 rpm, supernatant was removed, and microspheres were washed in PBS and resuspended in HBSS. Cortical and hippocampal sections were incubated with 2.45 × 10^6 microspheres (in a volume of 500 μl of HBSS) at 37°C for 1 h. Lastly, sections were intensively washed with 0.1 M PBS (3 × 20 min) and finally fixed with 4% PFA for 1 h. After fixation,

immunostainings for microglia using an anti-Iba1 antibody (Wako Pure Chemicals) was conducted. At first, a permeabilisation buffer containing 2% Triton X-100, 2% bovine serum albumin and 10% normal donkey serum in 0.1 M phosphate buffer (pH 7.4) was applied for 4 h, which was followed by the incubation with the donkey anti-goat Iba1 antibody (1:600; Wako Pure Chemicals) in a dilution buffer (1:10 of permeabilisation buffer in 0.1 M PBS, pH 7.4) at 4°C overnight. Thereafter, sections were incubated with the secondary antibody Alexa Fluor® 488-labeled donkey anti-goat antibody (Dianova, Germany; 1:200 in dilution buffer) for 2h at RT. After washing, slices were mounted in Aqua-Poly/Mount (Polysciences). Confocal laser scanning microscopy was performed on a Leica TCS SPE using a 20X oil immersion objective. We acquired 20 μm thick z stacks at 1 μm intervals beginning from the surface of the slices.

Data analysis to assess microglial phagocytic activity was performed using Imaris 6.3.1 (Bitplane, Zürich, Switzerland). The Iba1-positive volumes of high-resolution SPE confocal microscopy stacks were 3D surface rendered by application of a threshold value of 40 and a background subtraction value of 90 μm. Adjustments of the settings were done with blinded samples. Microspheres were detected as spots and counted automatically by the "Split into surface object"-plugin. All beads having their center located within a given rendered Iba1 volume were considered to be phagocytosed by microglia. The phagocytic index was calculated as followed: $n_{PM}*10^4/ V_{Iba\text{-}1}$ where n_{PM} is the total number of phagocytosed microspheres and $V_{Iba\text{-}1}$ the Imaris-rendered volume of Iba1 fluorescence in μm^3. For statistical analysis, GraphPad Prism 6 (La Jolla, USA) was used. We performed statistical analysis applying one-way ANOVA followed by a posthoc Tukey test for multiple comparisons of both sexes. To illustrate the method, we added a video in the supplementary material section.

Flow cytometry analysis

13 week old male and female animals were perfused under deep anesthesia transcardially with 1x Phosphate Buffered Saline (PBS) and brains were removed. The hippocampus and frontal cortex were extracted and homogenized in dissection buffer (1x HBSS (Thermo Scientific), 45% glucose, 1M HEPES) and cell pellets were resuspended in 25 mL of 22% Percoll (GE Healthcare, Little Chalfont, UK). 5 mL PBS was added as a layer on top. Centrifugation was performed for 20 min at 950 g with full acceleration and no breaks. Myelin cloud and rest of the supernatant were removed. Pellets were resuspended in ice-cold FACS buffer and filtered with 70 μm cell strainer. The cell pellet was resuspended at 10^6 cells/ml and stained with dye-coupled monoclonal anti-mouse antibodies: CD45, CD11b, MHCI, and MHCII. (eBioscience, San Diego, USA) for 20 min at 4°C. After the incubation, cells were immediately acquired on a LSRII flow cytometer (BD Bioscience, San Jose, USA) and data was analyzed using FlowJo v10 software (Tree Star). Statistical analysis were performed applying two-way repeated-measures ANOVA followed by Bonferroni post hoc test for comparisons of both sexes. Significance was defined as * $p < 0.05$; ** $p < 0.01$; *** $p < 0.001$.; **** $p < 0.0001$. All error bars are given as the standard error of the mean.

Magnetic cell sorting (MACS) of microglial cells

Under deep anesthesia, animals were transcardially perfused with ice-cold PBS. After decapitation, the brains were removed and frontal cortex and hippocampus were dissected in ice-cold Hank's balanced salt solution (HBSS, GIBCO, Invitrogen, Karlsruhe, Germany). Single cell suspension of hippocampus and frontal cortex were homogenized in dissection buffer (1x HBSS (Thermo Scientific), 45% glucose, 1M HEPES) and the pellets were resuspended in ice-cold percoll solution composed of percoll (GE Healthcare, Little Chalfont, Buckinghamshire, UK) and myelin gradient buffer, a layer of PBS was applied on top and centrifuged at 950 g, 4°C no brake and full acceleration. The cells were washed in ice-cold MACS-buffer (PBS, 0.5% bovine serum albumin, 2 mM EDTA) and stained with anti-mouse CD11b magnetic beads (Miltenyi Biotech, Bergisch Gladbach, Germany) at 4°C for 20 minutes. Due to limitation of cell number, three hippocampi were pooled and total cells were passed through large-sized MACS columns (Miltenyi Biotech, Bergisch Glabdach, Germany). The flow through was discarded and the cells were flushed out of the column in MACS buffer and pulled down by centrifugation. Cells were resuspended in either 1 mL TRIzol (Thermo Scientific, Schwerte, Germany) and snap frozen in liquid nitrogen and stored at −80°C for subsequent lysis for RNA extraction or put into PBS and subjected to protein extraction for the Proteomic analysis.

Purity analysis of CD11b+ MACS sorted cells using Flow Cytometry

CD11b+ MACS sorted brain and blood cells (see method section: MACS sorting of microglia) were resuspend in FACS buffer (2% FCS in PBS) and stained with dye-coupled monoclonal anti-mouse antibodies: CD45, CD11b, Ly6G, and Ly6C. (eBioscience, San Diego, USA) for 20 min at 4°C. After the incubation, cells were immediately acquired on a LSRII flow cytometer (BD Bioscience, San Jose, USA) and data was analyzed using FlowJo v10 software (Tree Star).

mRNA library preparation and sequencing

In order not to compromise the results just by mere cell number, the same amount of cells for each sex were used for RNA extraction. Total RNA integrity and quality was assessed with Agilent 2100 Bioanalyzer using an RNA 6000 Nano LabChip kit (Agilent Technologies, Ltd). In total, 16 strand-specific polyA enriched RNA libraries were prepared (four biological replicates for each treatment) using the KAPA Stranded mRNA Sample Preparation Kit according to the manufacturer's protocol (Kapa Biosystems, Wilmington MA, USA). Briefly, mRNA molecules were enriched from 50-250ng of total RNA using poly-T oligo-attached magnetic beads (Kapa Biosystems). Obtained mRNA was subsequently fragmented and the first-strand cDNA was synthesized using a reverse

transcriptase and random hexamers. Second cDNA synthesis was performed to generate double-stranded cDNA (dsDNA). Adenosines were added to the 3′ ends of dsDNA and adapters were ligated (adapters from NEB, Ipswich, MA, USA). Following the adaptor ligation, uracil was digested by USER enzyme from NEB (Ipswich, MA, USA) in a loop structure of adaptor. Adapters containing DNA fragments were amplified by PCR using NEB starters (Ipswich MA, USA). Library evaluation was done with Agilent 2100 Bioanalyzer using the Agilent DNA High Sensitivity chip (Agilent Technologies, Ltd.) Mean library size was 300bp. Libraries were quantified using a Quantus fluorometer and QuantiFluor double stranded DNA System (Promega). Libraries were run in the rapid run flow cell and were paired-end sequenced (2x100bp) on HiSeq 1500 (Illumina, San Diego, CA 92122 USA).

qRT-PCR validation of selected genes

For qRT-PCR validation of selected genes, CD11b+ MACS sorted cells were used for RNA extraction (see method section of MACS sorting and RNA extraction). After RNA extraction, first stranded cDNA synthesis was done with the SuperScript II reverse transcriptase (Invitrogen, Carlsbad, USA) using oligo-dT primers$_{12\text{-}18}$ (Invitrogen, Carlsbad, USA) according to the manufacturer's instructions. Quantitative real-time PCR reactions were performed in a 7500 Fast Real-Time thermocycler (Applied Biosystems, Carlsbad, USA) using the SYBR Select Master Mix (Applied Biosystems, Carlsbad, USA). The expression data was normalized to TBP gene expression for each sample. Following Primers were used for analysis: S100a8 forward 5′-CCGTCTTCAAGACATCGTTTGA-3′, S100a8 reverse 5′-GTAGAGGGCATGGTGATTTCCT-3′, S100a9 forward 5′-ATACTCTAGGAAGGAAGGACACC-3′, S100a9 reverse 5′-TCCATGATGTCATTTATGAGGGC-3′, Per1 forward 5′-TGGCTGATGACACTGATGCAA-3′, Per1 reverse 5′-CTCGTGTCCATTG GATTCATTG-3′, Enc1 forward 5′-ACCCTGCACGAGTGGTC-3′, Enc1 reverse 5′-GGACAGGTGGCCGGTACAGT-3′, Ppp6c forward 5′- ACACAGGTGTATGGATTTTATGATG −3, Ppp6c reverse 5′- TGAGCATATCAAAAACTTTGGTACAG −3′.

Protein extraction and Mass spectrometry analysis

Microglia primary cells from four different male/female mice were pelleted in PBS. The samples were solubilized in Laemmli buffer (LB) and subjected to SDS-PAGE. The proteome was focused in one gel band and was processed as described elsewhere (Shevchenko, Tomas et al., 2006, Kanashova, Popp et al., 2015), with the modification of using an automated HTS PAL system (CTC Analytics, Switzerland). Peptides were extracted, purified and stored on reversed-phase (C18) StageTips (Rappsilber et al., 2007). After elution, the peptides were lyophilized and resuspended in 0.1% Formic Acid / 3% Acetonitrile. Protein analysis by label-free quantification (LFQ). Peptides were then separated in a nano EasyLC 1200 (Thermo Fisher Scientific) with a 0.1 × 200 mm MonoCap C18 HighResolution Ultra column (GL Sciences, Japan) at a flow rate of 300 nL/min with a gradient from 5 to 95% B in 360 min. The UHPLC was coupled online to an Orbitrap Q Exactive mass spectrometer (Thermo Fisher Scientific) for mass spectrometry analysis. The mass spectrometer was set to acquire full-scan MS spectra (300–1700 m/z) at a resolution of 17,500 after accumulation to an automated gain control (AGC) target value of 1 × 106 and maximum injection time of 20 ms, and was operated in a data-dependent acquisition mode, selecting the ten most abundant ions for MS/MS analysis, with dynamic exclusion enabled (20 s). Charge state screening was enabled, and unassigned charge states, and single charged precursors were excluded. Ions were isolated using a quadrupole mass filter with a 2 m/z isolation window. A maximum injection time of 60 ms was set. HCD fragmentation was performed at normalized collision energy (NCE) of 26%. The recorded spectra were searched against a mouse database from Uniprot (January 2017) using the MaxQuant software package (Version 1.5.2.8) (Cox and Mann 2008) with fixed modifications set to carbamylation of cysteines and variable modifications set to methionine oxidation. Peptide tolerance was 20 ppm and the minimum ratio for LFQ was set to 2. The false-discovery rate was set to 1% on protein and peptide level. Statistical analysis of the dataset was performed using both R-statistical software package (version 3.4.1) and Perseus software (version 1.6.0.7). For data analysis, first, proteins that were only identified by site or were potential contaminants were excluded. Only those proteins that were found in at least three biological replicates for either female or male microglia were used for column wise imputation from a normal distribution and subsequent statistical analysis. For this a two-sample t test was performed with a permutation based FDR < 0.01. Abundance changes with a p value < 0.05 and a minimum fold change of 2 were considered significant (Table S4). The GO analysis was carried out as described above (for mRNAs): significantly, differentially regulated proteins (corresponding Ensembl gene IDs) were used as target and all other proteins captured by proteomics experiment were considered as a background. Protein IDs that matched several gene IDs were removed from the analysis.

QUANTIFICATION AND STATISTICAL ANALYSIS

Bioinformatic analysis of the RNA seq data

Paired-end RNA-Seq reads were mapped to the mouse reference genome GCRM38/mm10 with STAR (2.4.2a-foss-2015a) using the following parameters '—outFilterMultimapNmax 20 —alignSJoverhangMin 8 —alignSJDBoverhangMin 1 –outfilterMismatchNmax 999 —outFilterMismatchNovelLmax 0.04 —alignIntronMin 20 —alignIntronMax 10^6 —alignMatesGapMax 10^6' (Dobin, Davis et al., 2013). Mapped read pairs were assigned to genes with featureCounts (subread/1.4.6-p5) using '-t exon -g gene_id -s 2′. We used gencode version M6 (Ensembl 81) mouse genome annotation (Liao, Smyth et al., 2014). Alternative scaffolds were removed from the analysis. To identify differentially expressed genes within different conditions, we used R/Bioconductor DeSeq2 ((Love, Huber et al., 2014) version 1.16.1). The analysis was carried out with DeSeq2 default parameters, using raw read counts. Gene ontology (GO) analysis for differentially expressed mRNAs was performed with topGO (version 2.28.0), gene ontology tool, using

the 'elim' algorithm and nodes = 5. Significantly (adj. P value < 0.01) differentially regulated (|LFC| > 0.5) genes were used as target and all other protein coding genes as a control. For the comparison with P60 data, we downloaded all available fastq files from ENA (http://www.ebi.ac.uk/ena): SRR5642466, SRR5642467, SRR5642468, SRR5642469, SRR5642470, SRR5642471, SRR5642472, SRR5642497, SRR5642498, SRR5642499, SRR5642500, SRR5642501. All samples were processed in exact same way as our 13-week data.

Statistical Analysis

To assess statistical differences, we used Prism 6 for Windows (Graphpad Software, La Jolla, CA, USA). For the Density and soma size analysis, a two-way repeated-measures ANOVA followed by Bonferroni post hoc test was performed. For the electrophysiological analysis we used students' t test with Welch's correction; for the Phagocytosis Analysis we used one-way-ANOVA with Turkeys post hoc test and for the FACS data analysis we used a Students t test. Significance was defined as * $p < 0.05$; ** $p < 0.01$; *** $p < 0.001$.; **** $p < 0.0001$. All error bars are given as the standard error of the mean.

DATA AND SOFTWARE AVAILABILITY

The deep sequencing data have been deposited in Sequence Read Archive under BioProject: PRJNA408225 accession ID: SRP118459. The mass Spectrometry raw data have been deposited in the ProteomeXchange (via MassIVE) under ID codes PXD008114.

Cell Reports, Volume *24*

Supplemental Information

Transcriptional and Translational Differences of Microglia from Male and Female Brains

Dilansu Guneykaya, Andranik Ivanov, Daniel Perez Hernandez, Verena Haage, Bartosz Wojtas, Niklas Meyer, Meron Maricos, Philipp Jordan, Alice Buonfiglioli, Bartlomiej Gielniewski, Natalia Ochocka, Cagla Cömert, Corinna Friedrich, Lorena Suarez Artiles, Bozena Kaminska, Philipp Mertins, Dieter Beule, Helmut Kettenmann, and Susanne A. Wolf

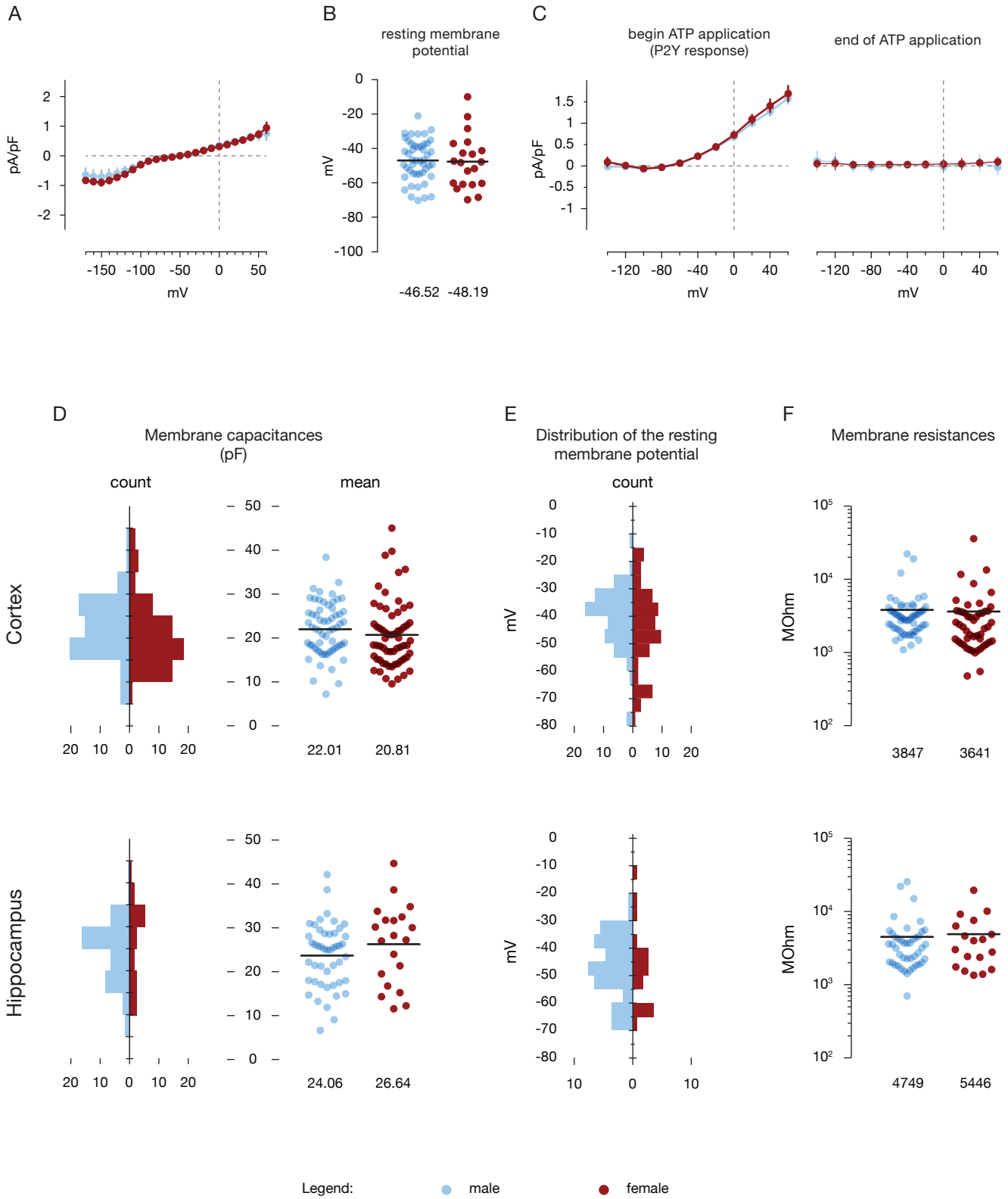
A
pA/pF
mV
B
resting membrane potential
mV
-46.52
-48.19
C
begin ATP application (P2Y response)
end of ATP application
pA/pF
mV
D
Membrane capacitances (pF)
count
mean
Cortex
22.01
20.81
Hippocampus
24.06
26.64
E
Distribution of the resting membrane potential
count
mV
F
Membrane resistances
MOhm
3847
3641
4749
5446
Legend:
male
female

Supplemental Figure 1. Passive membrane properties of patched microglia, Related to Figure 2

Membrane currents were recorded from microglia located in acute hippocampal and cortical slices while clamping the cell to -70 mV as described in figure 2. (A) The average current density (pA/pF) to voltage (mV) relationship was obtained from hippocampal microglia. Microglia derived from male mice show no significant difference in baseline inward and outward conductances compared to female. (B) Distribution of reversal potentials from male and female microglia. Microglial cells derived from female mice showed no significant difference in the resting membrane potentials compared to male. Average values indicated at the bottom. (C) To construct the current density to voltage relationship (pA/pF to mV) of the ATP-activated current component, values before ATP application were subtracted from currents at the peak of the response of the induced inward current and the peak of the induced outward current as indicated in figure 2. No significant differences in the reversal potential as well as in the inward or outward conductance upon ATP application were observed between sexes. 3 animals per group were used, and the number of recorded hippocampal microglia was for males n = 19 and for females n = 15. (D) Summary of the membrane capacitance represented as scatter plots and histograms reveals no significant differences between male and female both in hippocampus and cortex. (E) Distribution of the reversal potentials shown as averaged histograms of microglia from male and female animals. (F) Scatter plot depicting the membrane resistances shows no significant differences between male and female in both regions.

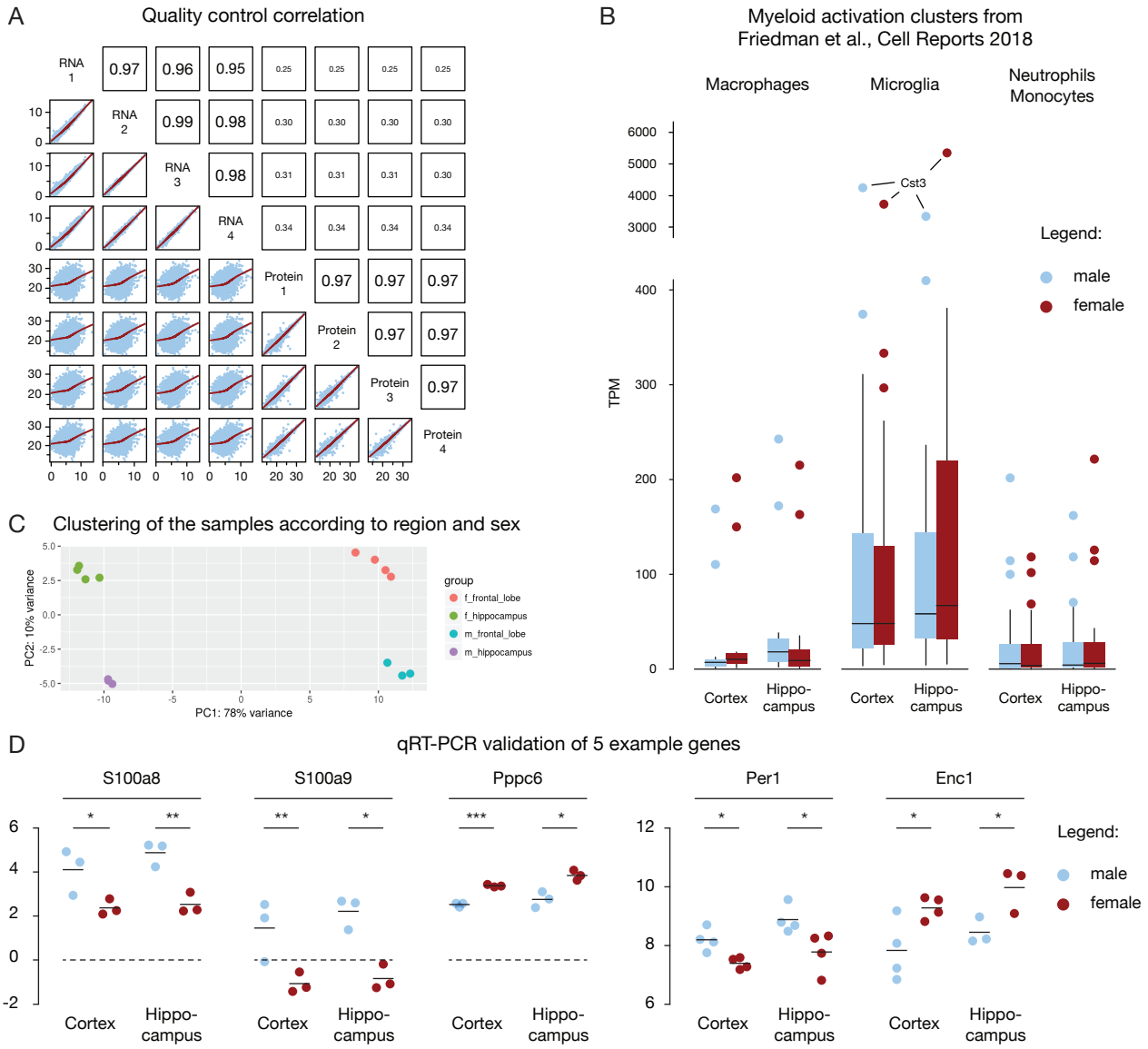

Supplemental Figure 2. Sex dependent transcriptome profile, Related to Figure 4

(A) Cross-comparison of RNA (from hippocampus) and protein (total brain) expression levels: The X and Y axes of the scatter plots represent the gene log2 TPMs or log2 iBAQ intensity in each sample. Red lines are the running averages. Pearson's correlation coefficients for each of the comparisons are depicted in the upper panels of the diagonal. The correlation is the highest within RNA replicates and within protein replicates, whereas correlation between proteins and RNA is low. (B) Friedman et al., (Cell Reports 2018) identified co-regulated gene modules from transcriptional profiles of CNS myeloid cells in different mouse models. The analysis incorporated RNA sequencing data from more than 300 expression profiles across different brain disease models, developmental stages, brain regions and myeloid cell types. In particular, clustering of normalized gene expression values identified microglia, macrophage and neutrophil/monocyte gene modules. To check for possible contamination in our sequencing data we compared the gene expression values in these modules. Box plots show the distribution of gene expression in different myeloid activation modules. Y-axis is TPM: (transcript per million). Supplementary table 1 contains genes in each three modules. (C) Principal component analysis of RNA-Seq samples. (D) qRT-PCR in freshly isolated microglia from hippocampus and cortex. Delta Ct values of 5 selected differentially expressed genes between male and female samples. Data are shown as the delta ct compared with endogenous TBP as mean ± s.e.m. At least 3 mice per n and three n per group were analyzed. Significant differences were analyzed by an unpaired Student t test (*P < 0.05, **P < 0.01, ***P < 0.001).

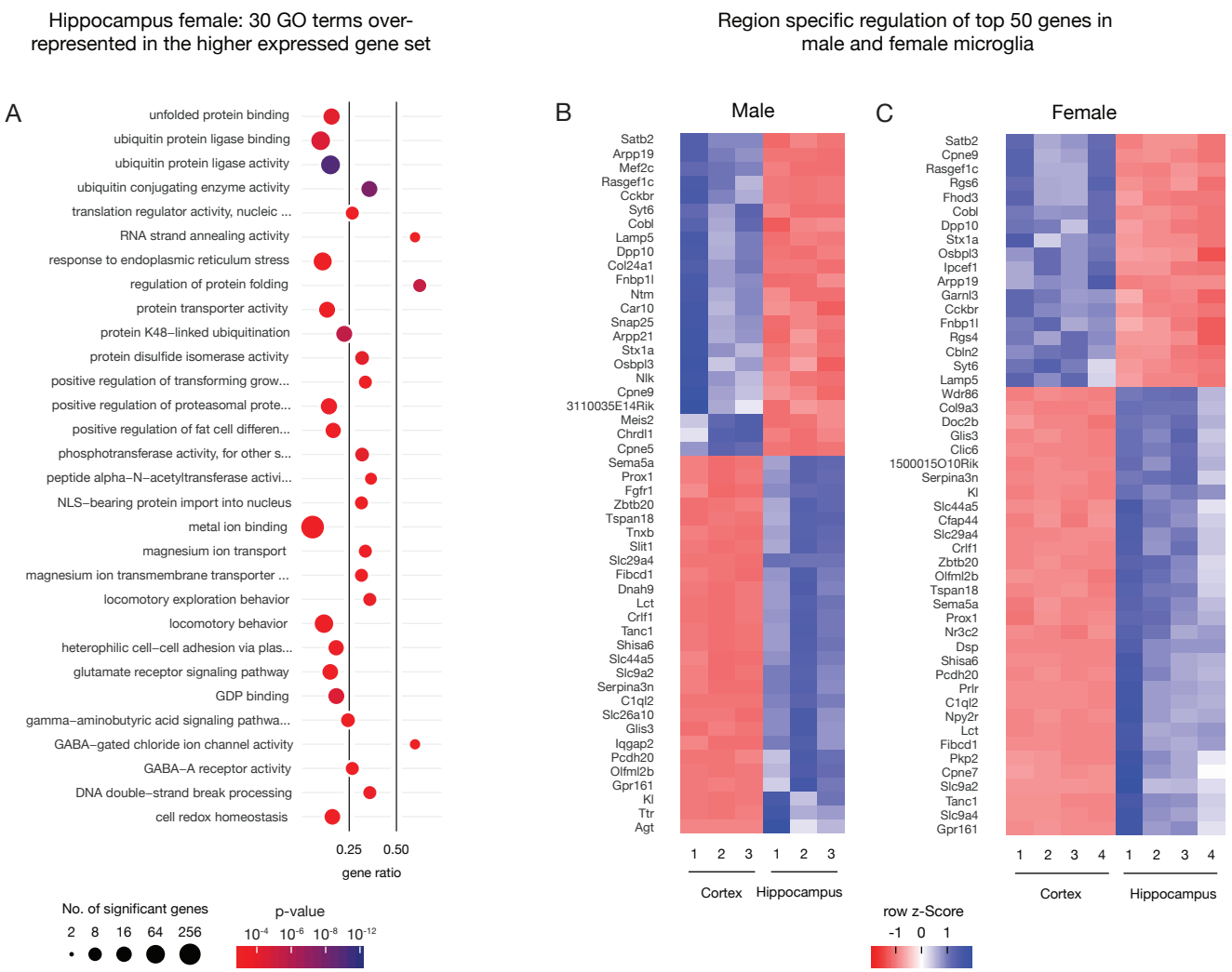

Supplemental Figure 3. Sex dependent transcriptome profile, Related to Figure 5

(A) Gene ontology analysis of hippocampus female: top 15 molecular functions and top 15 biological processes. (B-C) Heat maps show the top 50 (sorted by adj. p-value) differentially regulated genes for each of the comparisons in hippocampus vs. cortex in male and female samples. Z-scores are calculated per gene from TPM (transcript per million) values of each replicate.

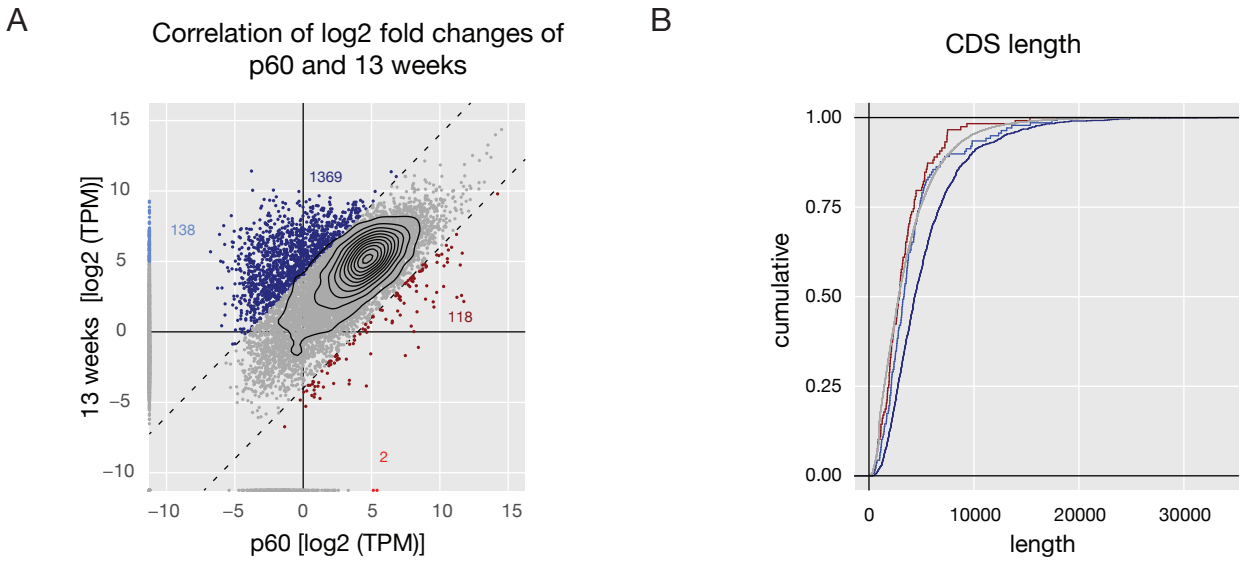

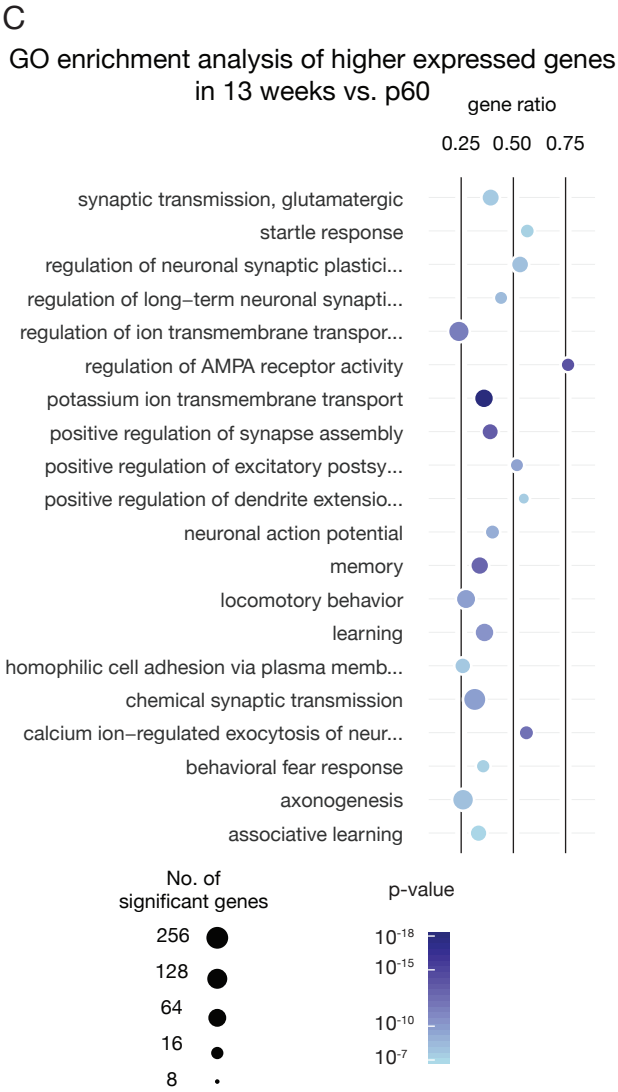

Supplemental Figure 4. Comparison of male hippocampal transcriptome profile at 13 weeks with P60 data set (Hanamsagar et al. 2017), Related to Figure 4

(A) Figure shows the comparison of the mean (over replicates) gene TPM values between our RNA-Seq (male hip-pocampus, 13-week-old mice) samples and RNA-Seq samples from Hanamsagar et al. study (male hippocampus, P60). Hanamsagar et al. measured the expression levels of total RNA: SRR5642497, SRR5642498, SRR5642499, SRR5642500 (in total ~14 million single ended reads, with 86-92% unique mappability). We sequenced polyA se-lected RNA, with 3 replicates (in total ~56 million paired end reads, with 93-94% unique fragment mappability). We detected 1369 genes (dark blue) with 16-fold higher TPMs in our data, while in Hanamsagar et al., only 118 (dark red). We also detected 138 highly expressed genes (log2_TPM > 5, blue) in our data that had zero read counts in P60. In P60 study, only two genes were highly expressed (log2_TPM > 5, red) and had no read counts in our study. (B) Comparison of the mRNA length between different groups of genes from the upper scatter plot. (C) Gene On-tology analysis of the blue and dark blue subpopulation of genes from the upper scatter plot. X-axis is the ratio between significantly differentially regulated genes and the total number of genes in that GO category. The X-axis and the size of the plots are analogous to Figure 5.

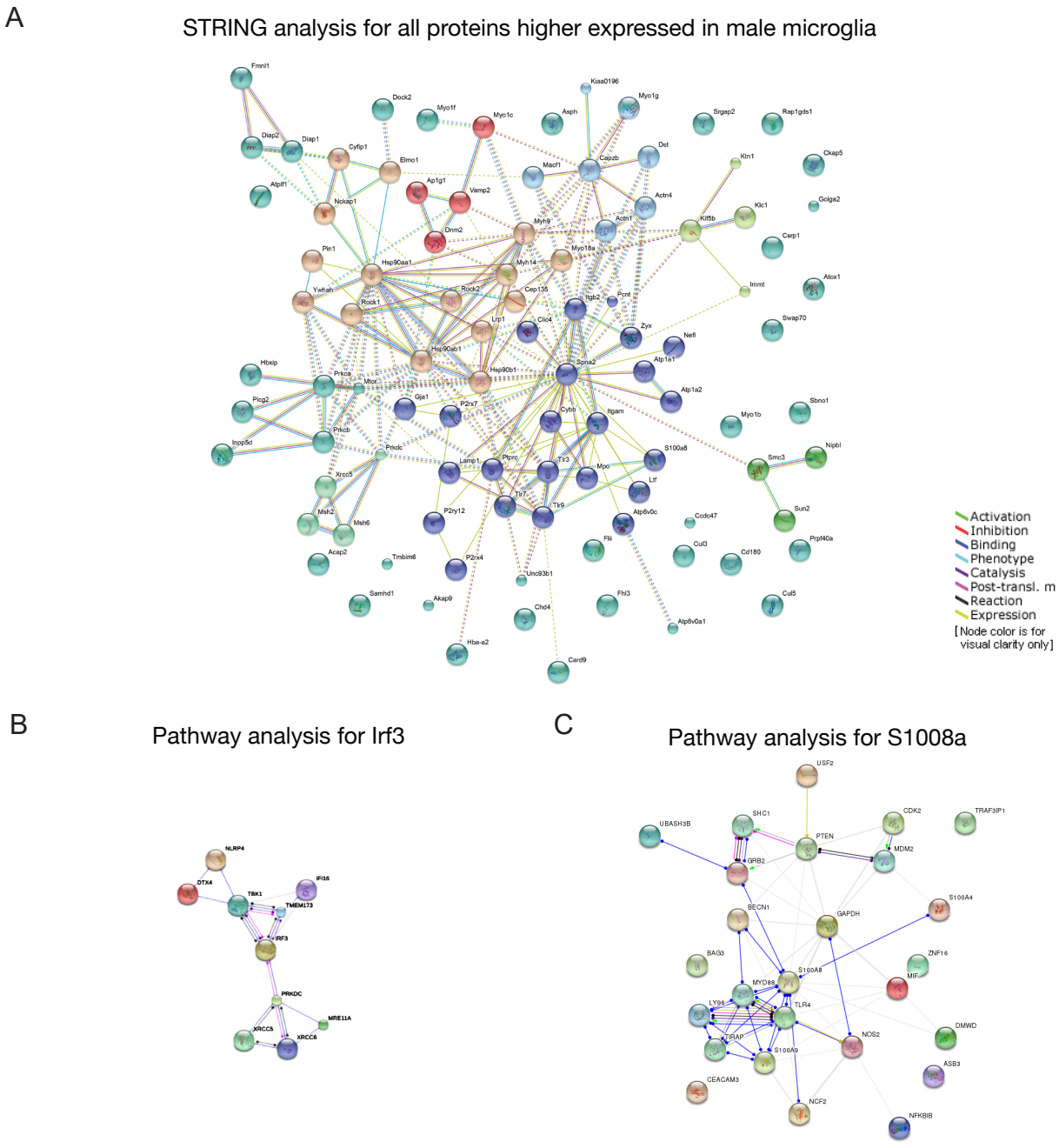

Supplemental Figure 5. Pathway analysis for proteins expressed at significantly higher levels in male microglia, Related to Figure 6

Search Tool for the Retrieval of Interacting Genes/Proteins (STRING) pathway analysis of proteins. (A) Network of all proteins expressed at significantly higher level in male microglia from Mass spectrometry analysis. Each color represents different clusters (k-means clustering). The settings for the relationship between those proteins are the evidence as network meaning, and found in experiments or databases as active interaction sources. (B-C) STRING pathway analysis of specifically picked proteins that are involved in microglia regulation. Each color represents a different pathway related to microglia. Individual proteins are labeled by gene name, and thicker lines represent more evidence of association. (B) Irf3 related pathway: Irf3 was one of the few genes expressed higher level in the proteomic female data set. However, Prkdc and Xrccr5 were expressed at higher level in the male microglia proteo-me. (C) S1008a related pathway. This was one of the few genes expressed at higher level in the male data set from proteomic and transcriptomic analysis.

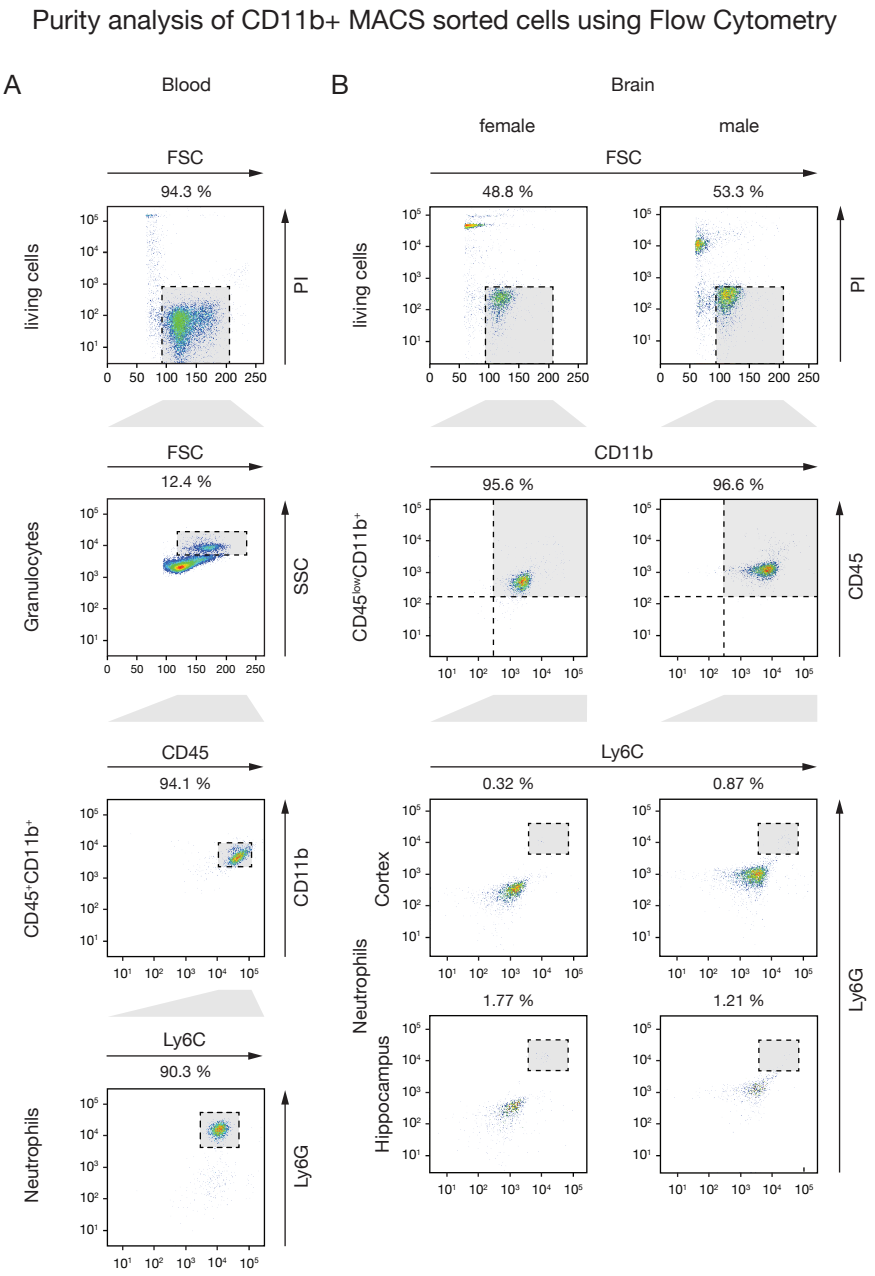

Supplemental Figure 6. Purity of CD11b+ cell population, Related to Figure 4 and 5

We show here a representative flow cytometry analysis of CD11b+ MACS sorted cells for the purity of the CD11b+ cell population. Blood samples were used to define the position of Ly6G+ neutrophil population in the gating strate-gy. CD11b+ cells were further defined in sub-populations using the expression of Ly6G (neutrophils) and Ly6C (monocytes). Less than 2% of the CD11b+ cell population are Ly6G positive in both male and female hippocampus and cortex.